CHALMERS

Heavy vehicle path stability control for collision avoidance applications

Master's Thesis in the Automotive Engineering program

ARMAN NOZAD

Department of Applied Mechanics
Division of Automotive Engineering and Autonomous Systems
CHALMERS UNIVERSITY OF TECHNOLOGY
Göteborg, Sweden 2011
Master's Thesis 2011 :45

MASTER'S THESIS 2011

Heavy vehicle path stability control for collision avoidance applications

Master's Thesis in the Automotive Engineering program

ARMAN NOZAD

Department of Applied Mechanics
Division of Automotive Engineering and Autonomous Systems
CHALMERS UNIVERSITY OF TECHNOLOGY
Göteborg, Sweden 2011

Heavy vehicle path stability control for collision avoidance applications

Master's Thesis in the Automotive Engineering program
ARMAN NOZAD

Master's Thesis 2011
ISSN 1652-8557
Department of Applied Mechanics
Division of Automotive Engineering and Autonomous Systems
Chalmers University of Technology
SE-412 96 Göteborg
Sweden
Telephone: + 46 (0)31-772 1000

Cover:
VOLVO PH12 truck which is close to the vehicle modelled in this study.

Department of Applied Mechanics
Göteborg, Sweden 2011

Heavy vehicle path stability control for collision avoidance applications

Master's Thesis in Automotive Engineering program
ARMAN NOZAD
Department of Applied Mechanics
Division of Automotive Engineering and Autonomous Systems
Chalmers University of Technology

Abstract

The current state of the art for Advanced Driver Assistant System (ADAS) in heavy trucks is based on pure braking interventions for rear-end collisions on highways and rural roads. In order to expand the scope to more general target scenarios, it is necessary to integrate braking and steering for more advanced interventions. The investigated target scenarios, which will cover not only rear-end collision, but also lateral conflicts and head-on collisions, are developed and prioritized based on accident statistics. For advanced interventions not only the speed of the truck but also the path should be under control. In fact the appropriate path controller should be applicable to various target scenarios and robust to variations in loading conditions. The overall goal of this work is to develop a path controller for a heavy vehicle based on integrated braking and steering, for collision avoidance application in the prioritized target scenarios.

To determine the potential of various actuator configurations to avoid the collision, an optimal control problem is formulated and solved for each scenario. The solution provides the requirements for the actuators and a bench mark for the developed optimal path controller. For vehicle implementation a robust controller which is capable of dealing with disturbances and uncertainties is needed.

The performance of the path controller in each target scenario and the sensitivity to key parameters is studied by performing the simulation on a detailed vehicle model. The target scenarios will be further prioritized based on the performance and robustness of the integrated braking and steering path controller.

As a result of this work, a path stability controller which is capable of integrating the steering and braking actuators during the manoeuvre will be provided. Therefore a robust path controller for Advanced Driver Assistant System can be provided which can handle not only rear end collision scenarios but also head-on and lateral conflicts for heavy trucks. This work can be a new constructive step in Heavy truck active safety and autonomous collision avoidance manoeuvre that extends the area in which active safety system participate to reduce the amount of accidents as much as possible.

Key words: Path stability control, Collision Avoidance, Active safety, Integrated steering braking.

Contents

Preface

This study deals with the design of a path stability controller for heavy vehicles in collision avoidance applications. The study has been carried out from January 2011 to July 2011. The work is a part of Interactive project which is financed by European Union. The work is mainly performed at Vehicle dynamics group, Applied mechanics department, Chalmers University of Technology, Göteborg, Sweden.

This part of the project (INCA) has been carried out with Mathias Lidberg as supervisor and VOLVO Technology Corporation as the project leader. I would like to appreciate Mathias Lidberg because of his help and endless support all along the project. I would also like to thank Lars Bjelkeflo and Mansour Keshavarz for their cooperation and involvement.

Göteborg July 2001

Arman Nozad

Notations

Uppercase Letters

C_ϕ	Roll damping of the
$C_{\phi,1}$	Roll damping of first axle
$C_{\phi,2}$	Roll damping of second axle
$C_{\phi,3}$	Roll damping of third axle
$F_{x,n}$	Longitudinal force on n^{th} wheel
$F_{y,n}$	Lateral force on n^{th} wheel
F_{dyn}	The force corresponding to dynamical condition
$F_{z,i,stat}$	Static load on i^{th} axle
$F_{z,n,stat}$	Static load on n^{th} wheel
I_{xx}	Vehicle moment of inertia around x axis
$I_{xx,s}$	Sprung mass moment of inertia around x axis
I_{zz}	Vehicle moment of inertia around z axis
K_ϕ	Roll stiffness
$K_{\phi,1}$	Roll stiffness of first axle
$K_{\phi,2}$	Roll stiffness of second axle
$K_{\phi,3}$	Roll stiffness of third axle
$K_{\phi,2+3}$	Roll stiffness of tandem axle
L	Distance between the first and the second axle
L_1	Distance between CG and the first axle
L_2	Distance between CG and the second axle $(L - L_1)$
L_3	Distance between CG and the third axle $(L + L_{bs} - L_1)$
L_e	Equivalent wheel base;

L_{fo}	Front overhang
L_{max}	Total length of the truck
L_{ro}	Rear overhang ($L_{max} - L - L_{bs} - L_{fo}$)
L_t	Theoretical wheel base
M_z	Vehicle yaw moment
W	Track width of the truck
W_{max}	Total width of the truck
X	Longitudinal position in global coordinate system
Y	Lateral position in global coordinate system
$\Delta F_{z,i}$	Load transfer on i^{th} axle

Lowercase Letters

a_x	Longitudinal acceleration
a_y	Lateral acceleration
c_δ	Steering compliance
g	Gravitational acceleration
h	Height of centre of gravity (CG) from ground
h_1	Roll centre height of first axle
h_2	Roll centre height of second axle
h_3	Roll centre height of third axle
h'	Height of centre of gravity (CG) from roll centre (RC)
i	Index number of axles starting from front to rear
i_s	Steering gear ratio
l_n	Longitudinal position of n^{th} wheel in the coordinate system fixed to the vehicle
m	Vehicle mass

m_s	Sprung mass
m_u	Unsprung mass
n	Index number of wheels starting from front and left (1) to rear and right (6)
v_x	Longitudinal speed of the vehicle
v_y	Lateral speed of the vehicle
w_n	Lateral position of n^{th} wheel in the coordinate system fixed to the vehicle

Greek Letters

α	Slip angle
α_m	Slip angle for which maximum lateral force is generated
δ_n	Wheel angle of n^{th} wheel
ε_{n}	Roll steer coefficient of n^{th} wheel
μ_1	The first coefficient in adhesion calculations
μ_2	The second coefficient in adhesion calculations
σ_x	Longitudinal relaxation length
σ_y	Lateral relaxation length
ϕ	Roll angle
ψ	Yaw angle

1 Introduction

Traffic safety is a major problem for today's transportation. A lot of work has been done in the passive safety area where milliseconds after the initiation of crash are of importance. Nowadays, collision avoidance in the field of active safety is more prioritised. This study focuses on autonomous path and path stability control of passenger cars and heavy vehicles which may serve as a basis for active interventions, particularly intended for helping the driver in critical collision avoidance manoeuvres.

In one hand, pure application of the service brakes to avoid an accident (by stopping the vehicle before colliding with the obstacle in front) is insufficient at relative high speeds. On the other hand, using only differential braking to steer the vehicle away from the obstacle in front is not feasible for a collision avoidance manoeuvre on the limits, since if this system is used, the sufficient amount of lateral forces will be built up when the vehicle yaw rate increases up to certain level thus making it a very slow response. Therefore the steering intervention comes into play in order to avoid accidents where the handling limits of the vehicle should be utilised as much as possible.

1.1 Problem description

A very general definition of the problem treated here is the question of how to keep a three-axle-truck autonomously on a desired escape path (on the limits). However, this is too general especially the number of solutions and/or combination of them is concerned; therefore the problem has to be narrowed down. In this study, main focuses are on:

- Path planning
- The type of actuation (steering, braking or their integration)
- The control algorithm

which will make "the path following on the limits" to be realised.

Possible and feasible actuation solutions for this study can be listed as follows:

- Pure front axle steering
- Pure braking
- Front axle steering + braking (differential braking and/or service braking)
- Front axle steering + braking (differential braking and/or service braking) + tag axle steering.

The evaluation criteria for various settings of the controller are given as follows according to the priority:

- All wheels must remain in contact with the road: This is important to be able to carry out the simulation from the beginning until the end.
- The lateral deviation from the reference path at the point where the obstacle is located should be as small as possible: this is important in order not to impact the obstacle as the desired path is designed so that the vehicle will follow it with small lateral deviations and avoid the obstacle.

- The maximum path deviation should be as small as possible: This is especially important, for instance, in order for the vehicle not to depart from the road after the obstacle in front has been avoided.
- The steering control input should be as smooth (i.e. free of vibrations) as possible in order to hand over the control to the driver without a problem.

1.2 Limitations and simplifications

As in all studies, there are also simplifications, limitations and assumptions in this study as well. Some of them are related to the control system dynamics which are used to simulate the behaviour of the controlled vehicle, whereas the rest is about the vehicle chassis and tyre properties.

1.2.1 Vehicle chassis and tyre model

- Pitch dynamics is not modelled. In fact, yaw and roll motion together influence the pitch dynamics due to the gyroscopic effect. Longitudinal load transfer is calculated by assuming a rigid (i.e. suspension locked for pitch motion) vehicle and cross terms consisting of roll, yaw and their rates are not considered.
- Aerodynamic drag and the effect of possible side winds are not modelled.
- Suspension springs and dampers are assumed to behave linearly for the whole range of roll angles and roll rates.
- Elastokinematical features (e.g. lateral force steer and aligning moment steer) of the suspension are not considered when modelling the axles. For all the axles, only the roll steer (i.e. kinematical feature) is taken into consideration with a simple linear expression. The camber change in rigid axles due to roll of sprung mass (lateral load transfer) is relatively small, that is also neglected.
- In a tandem axle group, longitudinal force and torque on one axle (located on the tandem axle) actually influence the vertical load on the other axle due to the measures taken to distribute the load on each axle of the tandem group in a predefined ratio on uneven surfaces. Here, it is assumed that the torque reaction rods used to counteract additional vertical load transfer due to torques and longitudinal forces are designed properly so that they (almost) cancel that effect.
- The steering angles of the left and right front wheels (on the first axle) are assumed to be the same. The steering ratio is assumed to be constant. The lumped elasticity in the steering system is assumed to be linear.
- Ladder chassis is assumed to be rigid. In reality, truck chassis is made of so-called profiles with “open” cross-sections. Since those profiles are torsionally flexible and relatively rigid for bending, the overall chassis structure is easily twisted. This is sometimes desired for trucks to better suit the road profile. However, as can be expected, torsionally flexible ladder chassis affects the lateral load transfer, but its affect on load transfer is not considered.
- Tyre rolling resistance is neglected.

- A linear reduction is assumed for the adhesion coefficient between the tyre and the ground with respect to the increasing normal load. Moreover, the horizontal asymptote for tyre lateral force vs. slip angle characteristic is assumed to be 75% of the peak force.
- A linear change is assumed for the horizontal position of the tyre peak force vs. slip angle point.
- A first order differential equation with constant relaxation length is used to model tyre force build-up.
- Rotating wheels are not simulated in order not to take the combined slip into account. A friction circle is used to determine the lateral force generated by a tire in presence of a known longitudinal force.

1.2.2 Control system dynamics

- The entire desired path is estimated at the point of intervention.
- Only high μ environment: Simulations on a low μ surface requires a different tyre model.
- Steering actuator delays and dynamics are not modelled.
- The delays due to slack in brake system are ignored. Instead, brake system is assumed to be pre-charged so that the effect of slack in brake performance is minute.
- Analogue brake and steering actuators are assumed in the simulation (i.e. infinite resolution, infinite update frequency).

1.3 Literature review

An approach based on artificial potential fields is introduced by Gerdes and Rossetter [1] to assist the driver with lane keeping issue. They use superposed brake and steer interventions on the driver's input and achieve both safety and drivability using such a system.

Hiraoka et.al. [2] propose a path-tracking controller for a four wheel steering (4WS) vehicle based on the sliding mode control theory. By decoupling the front- and rear-wheel steering, an advantage is made in controlling the vehicle thus achieving more stability and more precision in path-tracking in comparison with 2WS. There are more robustness in stability against system uncertainties and perturbations.

An adaptive linear optimal control is employed by Thommyppillai et.al. [3] to drive the car at certain limits of handling. The advantages of using gain-scheduled adaptive control over a fixed-control scheme are shown in simulations of a virtual driver-controlled car.

Kritayakirana and Gerdes [4] describes the development of a race path-controller using integrated steering braking system designed to drive a vehicle autonomously to its limits on an uneven dirt surface. In order to mimic the driver's ability in using the friction estimation for controlling the vehicle on the limits while tracking the racing line, the controller is divided into sensing and control-lining parts. The sensing part imitates the driver, learning the track profile and sensing the environment during practice. Afterward the controlling part calculates

the feed forward command like a driver planning ahead. While driving, the feedback controller imitates the driver's car control abilities, making adjustments based on changing conditions.

Therefore the controller can be divided into four important parts, a path description, friction estimation, steering controller and slip circle longitudinal controller. a clothoid path is used to construct a desired path. In this paper a pre-knowledge of friction distribution obtained from a ramp steer is used. from knowing the curvature, the feedforward steering input can be calculated and the steering feedback based on lane-keeping adds the robustness to the controller. Knowing the curvature of the track the longitudinal feedforward controller calculates the amount of throttle and brake for a desired trajectory. Longitudinal feedback controller based on slip circle fulfils two purposes. First, it provides a longitudinal input that controls tire slip and secondly the slip circle controller ensures that the tires are operating at their limits. This approach can maximize the tire forces while effectively controlling the tire slip.

Kharrazi, S. [5] investigates the truck accident statistics due to lateral instability of the truck and also studies different combination of truck and trailer considering their effect on lateral stability of the truck.

Yang, D. [6] describes the method for benefit prediction of using specific brake system configuration on vehicle post impact stability control. The information about the benefit study is found useful for this thesis.

Bilen, Ö. [7] deals with the heavy truck modeling and simulation. Early stage of usecase prioritization is also available in this literature.

1.4 Approach

Autonomous path and path stability control is a challenging non-linear control problem with constraints. The performance is evaluated with respect to several aspects as indicated above for several use cases described in the next chapter. There are also several feasible actuation solutions. Therefore an optimal control based methodology is used to investigate the potentials of the actuators to perform the manoeuvre and also benefits of the collision avoidance in each manoeuvre. These manoeuvres are defined based on the use cases introduced in earlier parts of work where the investigation on various target scenarios is made. For each manoeuvre there might be cases that are the variants of the main manoeuvre. Consequently, Path stability control simulation is performed for three different manoeuvres. These simulations show how efficient the controller is for each Use-Case. The controller will be then implemented on the demonstration vehicle which is a passenger car from FFA and a truck from VOLVO 3P using rapid control prototyping.

2 Use-Cases

2.1 Definition

The truck target scenarios covered in deliverable 1.5 [8] represent approximately 40% of all accidents in the used accident data base. This means that there are many accidents which have not been included in the interactIVe target scenario analysis. The major part of these accidents consists of accidents with crossing traffic. Other large accident groups are (i) accidents where the truck is hit from behind and (ii) reversing accidents. These accidents are not included in the analysis, since there are other projects focusing on accidents in crossings (InterSafe2) and the accidents where the crash happens in the rear end of the truck are not considered to be in the scope of INCA.

Use-Case template in InteractIVe project is based on: (1) the narrative, (2) the sketch and (3) the sequence diagram. A use case may include several alternative flows of events, which represent different possible solutions to a similar problem. Alternative flows may include different possible interactions for similar use cases or an escalating sequence of events. Separate use cases should be defined when the corresponding target scenarios differ fundamentally.

2.2 Prioritization

Use-Case prioritization is done based on accident statistics, Use-Case complexity, optimal control results and path stability simulation results.

The accident scenarios can provide us with some information about how frequently each type of accident happens or how much injury or cost. Based on this an early prioritization is done on accident scenarios from previous stages of work.

Use-Case complexity is considering the possibility of modelling the manoeuvre and its environment as well as investigating the required complexity of the model and the controller to fulfil the requirements.

The prioritized Use Cases based on accident statistics and Use-Case complexity are as follow:

- Rear-End Collision Avoidance (RECA) : This use case deals with the situation in which the truck have a higher velocity than the car in front. The velocity of interest based on statistics is 40-80 km/h
- Run-off-road prevention on a straight road (RORP): This use case deals with unwanted departure of the vehicle from the lane due to e.g. drowsiness of the driver. The speed of interest is 80-90 km/h.
- Run-off-road prevention on a curved road (RORP): This use case deals with the vehicle driving on a curved road with a rather large radius. The lack of action from the driver departs the truck from the road. The speed of interest is 80-90 km/h.

Based on the prioritization of the use-cases above it follows that it is of interest to study braking, steering, and integrated braking and steering for collision avoidance manoeuvres defined by the use cases above.

The optimal control results in this report are used to investigate the performance of the various actuator configurations for collision avoidance application in order to find out whether a specific configuration can work for this manoeuvre or not.

The use cases will be further prioritized based on the path stability controller results in this report to investigate the efficiency of the path controller in each manoeuvre.

3 Collision avoidance optimal control

The heavy vehicle system dynamics model developed in Appendix A is a nonlinear multi input-output dynamic system. The control of the vehicle in collision avoidance manoeuvres for various actuator configurations such as braking, steering and integrated braking-steering is nontrivial. In order to determine the potential of various actuator configurations and to benchmark the collision avoidance path and speed controller, an optimal control problem is formulated and solved for a simplified vehicle model. For this purpose the dynamics of the vehicle is modelled as a point mass (particle model).

3.1 Particle model

The particle vehicle model depicted in Figure 3.1 has two degrees of freedom in horizontal plane OXY.

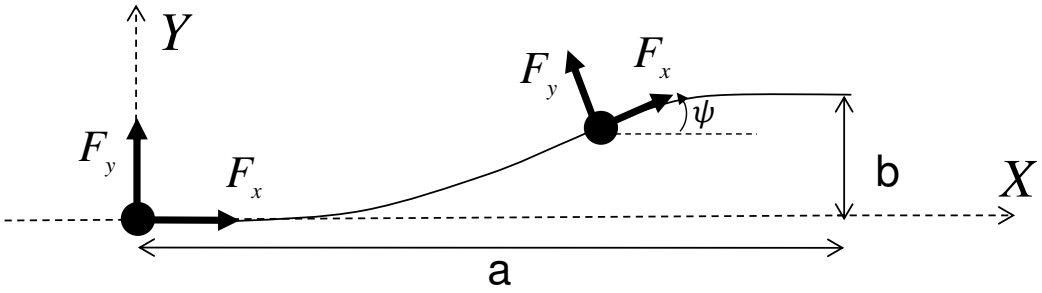

Figure 3.1 Schematic sketch of problem definition for particle model.

The driver and steering and braking actuators control the vehicle motion by demanding friction forces (steering F_y^D and braking F_x^D). The tire force generation in not instantaneous in real tires (see Appendix A), therefore tire relaxation lengths (σ_x, σ_y) are taken into account to model the force generation delay. The actual forces on tires are then F_x and F_y.

$$\frac{\sigma_x}{v_x}\dot{F}_x + F_x = F_x^D \tag{3.1}$$

$$\frac{\sigma_y}{v_x}\dot{F}_y + F_y = F_y^D \tag{3.2}$$

The friction forces are defined in local coordinate system Oxy while the particle motion is defined in global coordinate system OXY where the X axis is considered as the original track direction and Y axis is perpendicular to original track direction. The longitudinal and lateral distance during the collision avoidance manoeuvre are a and b, respectively.

The equations of planar motion for the vehicle particle model are:

$$m\ddot{X} = F_x\cos\psi - F_y\sin\psi \tag{3.3}$$

$$m\ddot{Y} = F_x \sin\psi + F_y \cos\psi$$

In order to satisfy the force limitation on the tires the steering and braking forces should stay within the friction circle.

$$(F_x)^2 + (F_y)^2 \leq (\mu m g)^2 \quad 3.4$$

The collision avoidance manoeuvre is defined by the initial and final conditions given bellow.

$$V_X(0) = V_{X0}, V_Y(0) = V_{Y0}, X(0) = X_0, Y(0) = Y_0, \quad 3.5$$

$$V_x(T) = V_{xT}, V_y(T) = V_{yT}, X(T) = X_T, Y(T) = Y_T \quad 3.6$$

The initial and final conditions mentioned above are used to define the boundary conditions for the collision avoidance manoeuvre. In rear end collision avoidance scenario for instance, the final global lateral velocity can be zero for the case when the coarse angle is considered as zero or a small value for the case considering non-zero coarse angle.

In order to generate a particle model which is capable of resembling the full vehicle model characteristics considering the tire limitations and rollover risk, some constraints should be applied to the particle model.

Considering the rollover risk, the lateral acceleration should stay below a certain limit.

$$|a_y| = \left|\frac{F_y}{m}\right| \leq a_{y,\max} \quad 3.7$$

The longitudinal acceleration can be limited in a similar way.

3.2 Optimal control problem

Introducing the state variables as $z = [X\ Y\ V_x\ V_y\ F_x\ F_y]^T$, the planar equations of motion (Equations 3.1-3.3) can be transformed to first order differential equations in state space form

$$\dot{z} = \begin{bmatrix} \dot{X} \\ \dot{Y} \\ \dot{V}_x \\ \dot{V}_y \\ \dot{F}_x \\ \dot{F}_y \end{bmatrix} = \begin{bmatrix} V_x \\ V_y \\ (F_x \cos\psi - F_y \sin\psi)/m \\ (F_y \cos\psi + F_x \sin\psi)/m \\ (v_x/\sigma_x)(F_x^D - F_x) \\ (v_x/\sigma_y)(F_y^D - F_y) \end{bmatrix} \tag{3.8}$$

Then general optimal control formulation in state space will be as follow:

Find the states $z(t)$ and controls $u(t)$ that minimize the objective function:

$$J(z,u) = c_0 z(0) + c_T z(T) + \int_0^T z^T Q z dt \tag{3.9}$$

Subjected to equations of motion from Equation 3.8

$$\dot{z}(t) = f(z,u) \tag{3.10}$$

where $u = [F_x^D, F_y^D]^T$ and boundary conditions

$$J_0 z(0) = z_0, J_T z(T) = z_T \tag{3.11}$$

together with constraints on states (e.g. position) and state derivatives (e.g. velocity and acceleration):

$$a_1 \le z(t) \le a_2 \tag{3.12}$$

constraints on controls

$$a_7 \le u \le a_8 \tag{3.13}$$

and quadratic constraints on controls

$$a_8 \le u^T R u \le a_9 \tag{3.14}$$

where the matrices J_0 and J_T are determined by Equation 3.5 and 3.6. Limitations on acceleration can be satisfied using Equation 3.12 and the friction circle is implemented using Equation 3.14.

The optimal control problem is also regularized and augmented by adding a small energy term to the objective function.

$$\tilde{J}(z,u) = J(z,u) + w\int_0^T u^T u\, dt \tag{3.15}$$

4 Path and speed control

A schematic sketch of a generic path and speed control system is provided in Figure 4.1. The control system includes blocks for path planning, decision algorithm, feed-forward and feedback. Each of these blocks is explained in following text.

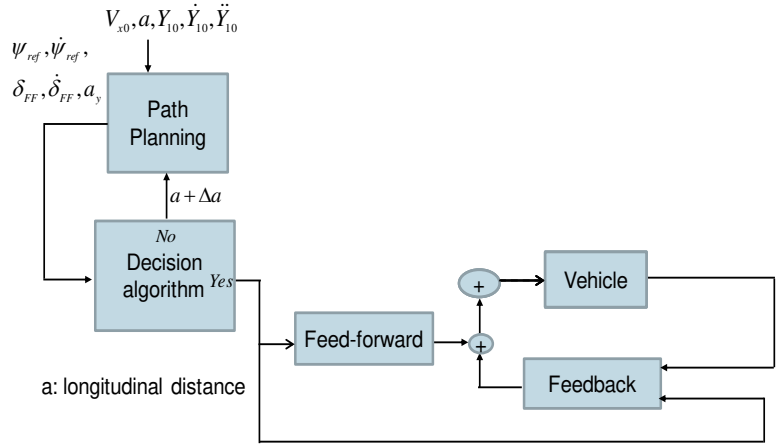

Figure 4.1 Schematic sketch of a generic path and speed control system.

4.1 Decision algorithm

The decision algorithm provides a feasible path by performing robust reference path optimization using the particle model defined in Section 3.1 with restrictions taken into account on steering angle, steering angle rate, lateral acceleration and wheel torque profiles. After finding a feasible path, the feed-forward steering angle will be provided as the output of the decision algorithm.

Since the manoeuvrability of a heavy vehicle on a high friction surface is limited by the roll over threshold rather than the tire capability to generate tire side forces, the lateral acceleration, should be kept bellow a certain limit obtained from Equation A 40.

$$\left|a_y\right| \le a_{y,\max} \tag{4.1}$$

Moreover, the handwheel angle and handwheel angle rate should be constrained due to mechanical limitations of actuators on steering angle and angular speed as well as driver's safety.

$$\left|\delta_{FF}\right| \le \delta_{FF,\max} \ , \ \left|\dot{\delta}_{FF}\right| \le \dot{\delta}_{FF,\max} \tag{4.2}$$

The required torque to the steering system should also be limited due to driver's safety and also the actuator limitations.

$$\left|T_w\right| \le T_{w,\max} \tag{4.3}$$

4.2 Path planning

4.2.1 Path planning requirements

The path planning should provide a continuous and smooth profile in advance of the intervention. This means that the position, velocity and acceleration profile should be continuous. Another important aspect is simplicity.

4.2.2 Piecewise polynomial

Considering the requirements on path planning, a piecewise polynomial has been chosen to satisfy the requirements.

$$Y_{ref,i}(X) = \sum_{j=0}^{n} C_{ij}(X - X_{i0})^{j}, i = 1,2,...,m \tag{4.4}$$

which is subject to the initial and final condition as follows

$$Y_1(0) = Y_{10}, \dot{Y}_1(0) = \dot{Y}_{10}, \ddot{Y}_1(0) = \ddot{Y}_{10} \tag{4.5}$$

$$Y_m(X(T)) = Y_{mT}, \dot{Y}_m(X(T)) = \dot{Y}_{mT}, \ddot{Y}_m(X(T)) = \ddot{Y}_{mT} \tag{4.6}$$

The entire path should be continuous and smooth which can be defined as follows.

$$\begin{gathered} Y_{ref,i,0} = Y_{ref,i-1,T}, Y_{ref,i,T} = Y_{ref,i+1,0}, \dot{Y}_{ref,i,0} = \dot{Y}_{ref,i-1,T}, \dot{Y}_{ref,i,T} = \dot{Y}_{ref,i+1,0}, \\ \ddot{Y}_{ref,i,0} = \ddot{Y}_{ref,i-1,T}, \ddot{Y}_{ref,i,T} = \ddot{Y}_{ref,i+1,0}, \\ i = 2,...,m \end{gathered} \tag{4.7}$$

4.2.3 Using a fifth order polynomial

Using one fifth order polynomial is appropriate to satisfy the requirements since it can constraint position, velocity and acceleration as initial and final condition. The fifth order polynomial is defined as follows:

$$Y_{ref}(X) = aX^5 + bX^4 + cX^3 + dX^2 + eX + f \ , \ m = 1, n = 5 \tag{4.8}$$

The following coefficients can be mentioned as an example for rear end collision avoidance escape path. This example is made for longitudinal and lateral displacement of 50 m and 3 m respectively.

Coefficients	***a***	***b***	***c***	***d***	***e***	***f***
Values	5.76e-8	-7.2e-6	2.4e-4	0	0	0

Table 4.1 An example of coefficients for fifth order polynomial

Except the three last coefficients that remain zero for all the cases in lane change path planning, all the other three values change by changing the longitudinal or lateral distance.
The fifth order polynomial with these coefficients is also shown in Figure 4.2.

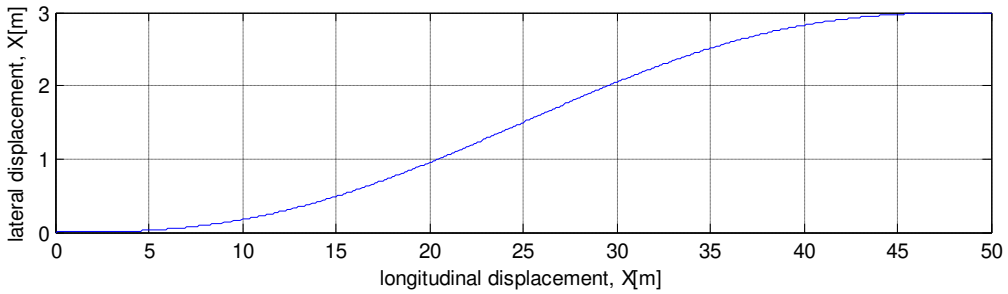

Figure 4.2 An example of a fifth order polynomial

The main advantage of the fifth order polynomial is that it provides a very smooth, continuous path profile. Therefore this path can be used for calculating the feed-forward steering as well as lateral acceleration required by the path. It is shown later in Figure 5.10 that the optimal and feed-forward steering profiles are comparable. Therefore it is logical to use the feed-forward steering profile which is based on the polynomial instead of running the optimal control online to obtain the optimal steering profile.

The fifth order polynomial is used for all the simulations in Chapter 5-6 with the heavy truck vehicle model. However this polynomial is not intended to be implemented real time. It is likely that a multiple lower order polynomials will be used in real time implementation. The order of the polynomial depends on the dynamics (e.g. filtering) of the truck and the actuators. As the conclusion to this part, it can be mentioned that the frameworks is quite flexible in using the polynomial and can easily change to any other polynomials with different order and multiple segments.

4.3 Path stability control design

The path stability controller objective is to minimize the path and heading angle error while maintaining the manoeuvrability and roll stability in order to perform the collision avoidance manoeuvre. Common actuators for this approach are steering and braking. Optimal control results for different actuators, shows more benefit in using the steering actuator in these cases (Section 5.1).

For a better efficiency and accuracy the path stability controller is designed in two parts, feed-forward steering which is the output of the path planning and decision algorithm is implemented in order to increase the responsiveness of the controller and feedback part that is operating on heading angle and heading angle rate error is used to compensate for inaccuracies. Since the vehicle response to steering and braking input is not instantaneous controlling the vehicle based on the reference point that it just passed cannot help the vehicle to follow the trajectory ahead especially if the vehicle is moving in high speed. Therefore, a preview time which provides a reference

point ahead of the vehicle at the distance depending on the velocity is implemented. The controller should operate within the bandwidth of steering actuator otherwise the actuator cannot provide what the controller requests for performing the manoeuvre. It is also assumed that the absolute position of the vehicle at each time which is used for braking stability control after the manoeuvre is known using a GPS or similar positioning system. The information about the heading angle, heading angle rate etc. are provided by build in sensors.

4.3.1 Feed-forward

The feed-forward steering angle is provided in advance based on the path provided by the path planning. The feed-forward output from path planning should satisfy the constraints in decision algorithm before being supplied to path stability controller. This steering angle is determined based on the path profile and assuming a two axle vehicle in steady state condition, defined in Section A3. Consequently a continuous and smooth steering profile is provided in advance.

The following equation is used to calculate the feed-forward steering input.

$$\delta_{FF} = \frac{L_e}{R} + K_u \frac{a_{y,ref}}{g} \tag{4.9}$$

where the reference lateral acceleration $a_{y,ref}$ is based on the reference path,Y_{ref} .and L_e is the effective wheelbase based on the static normal load on the $i-th$ axle, $F_{zi,static}$.

$$L_e = L + \frac{F_{z1,static}}{F_{z2,static} + F_{z3,static}}(l_3 - l_2) \tag{4.10}$$

4.3.2 Feedback

Feedback steering control is defined as a linear PD control on yaw angle error and yaw rate error. This part of the controller is applied in order to compensate the errors due to simplifications and inaccuracies. In order to compensate for the truck and tire dynamics, a preview time (t_p) is also used to apply the steering in advance.

$$\delta_{FB}(t) = K_p\left(\psi_{ref}(t+t_p) - \psi(t)\right) + K_d(\dot{\psi}_{ref}(t+t_p) - \dot{\psi}(t)) \tag{4.11}$$

where $\psi_{ref}(t+t_p)$ is the heading angle of the truck at the preview time ahead of the vehicle while ψ is the actual heading angle of the vehicle. The reference heading angle is directly calculated from the path profile.

$$\psi_{ref} = \tan^{-1}\left(\frac{dY_{ref}(X)}{dx}\right) \tag{4.12}$$

The total steering input of the vehicle will then be:

$$\delta = \delta_{FF} + \delta_{FB} \tag{4.13}$$

A schematic figure of the path stability controller is provided in Figure 4.3

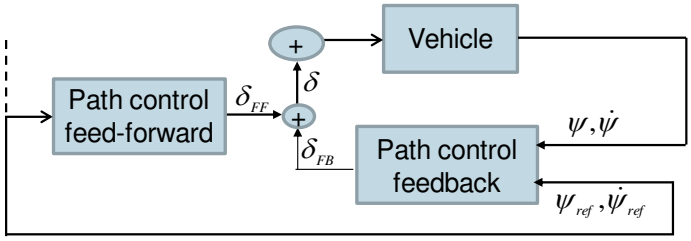

Figure 4.3 Schematic sketch of path stability controller.

4.4 Yaw control

In this study, the differential braking used for yaw control is divided into two parts:

- Turn in braking: Feed forward initial differential braking for compensating the delays due to dynamics of the steering system and vehicle yaw dynamics.
- Braking stability control: Differential braking as a feedback control on position after the lane change to stabilize the vehicle motion.

4.4.1 Turn in braking

Due to dynamics of the steering system, tire characteristics and vehicle yaw dynamics, the vehicle respond to the steering input is not instantaneous. In fact these dynamics operate very similar to a first order filter on the steering angle. Therefore there is a loss in steering performance while considering this effect in the simulation. In order to compensate this loss two different strategies can be considered.

- Increasing the preview time
- Using differential braking to increase the steering performance of the vehicle in very beginning of the manoeuvre in order to help the vehicle to follow the path with the same preview time that was used for the simulation without taking the system dynamics into account.

Since increasing the preview time is not favourable in designing the controller due to the fact that the controller is not supposed to get activated too early, the second approach is considered as the preferred approach. In this method the amount of braking force FD_{FF} on both wheels on either the left or right side of the truck will be provided as step input. The braking force is applied on side that is demanded by the reference curvature determined based on the reference path.

4.4.2 Braking stability control

The differential braking is used as a proportional controller on position error in order to compensate the offset due to inaccuracies, changes in the condition and faults at the end of the manoeuvre.

$$FD_{FB}(t) = -K_p\left|\left(Y_{ref}(t+t_p) - Y(t)\right)\right| \tag{4.14}$$

$$FD = FD_{FF} + FD_{FB} \tag{4.15}$$

The wheels used for differential braking are determined based on global lateral position error as indicated in Figure 4.4.

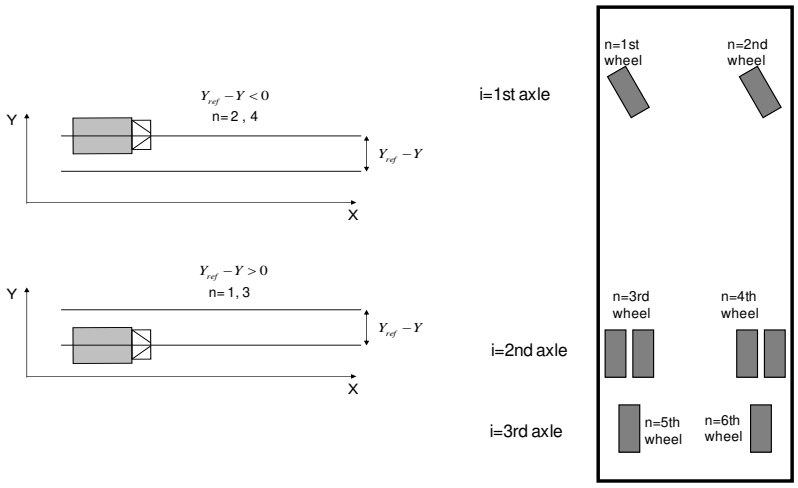

Figure 4.4 Schematic sketch of the braking stability control.

Schematic figure of the yaw controller is provided in Figure 4.5.

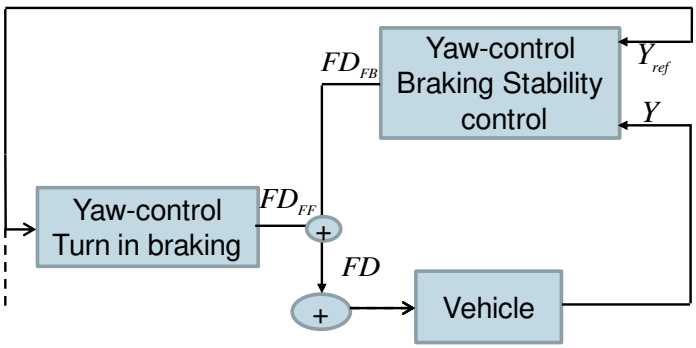

Figure 4.5 Schematic sketch of yaw controller.

4.5 Speed control

Very similar to reference path generation, a speed profile V_{ref} is generated by the path planning algorithm. The difference between the actual velocity of the vehicle and the reference velocity is defined as the velocity error. The speed control is then a feedback proportional controller acting on the velocity error which determines the amount of braking force that should be applied to the wheels in order to keep the reference speed.

The total braking force is distributed on axles proportional to the static load. The speed profile is trying to mimic the optimal control solution in a simplified way and it is not exactly the optimal control results. Therefore it is expected that the performance of this actuator is not as good as the optimal control.

The speed control is then defined as:

$$F_{FB}(t) = K_p\left(V_{ref}(t+t_p) - V(t)\right). \tag{4.16}$$

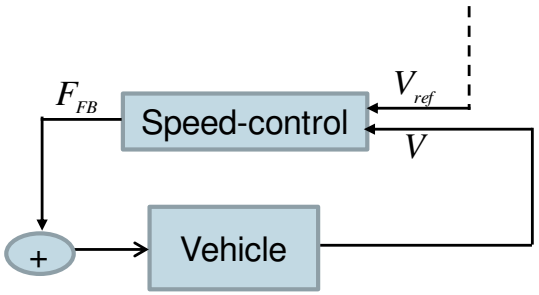

Figure 4.6Schematic sketch of speed controller.

4.6 Collision avoidance path and speed control system

The complete path and speed control system for collision avoidance application is provided in Figure 4.7.

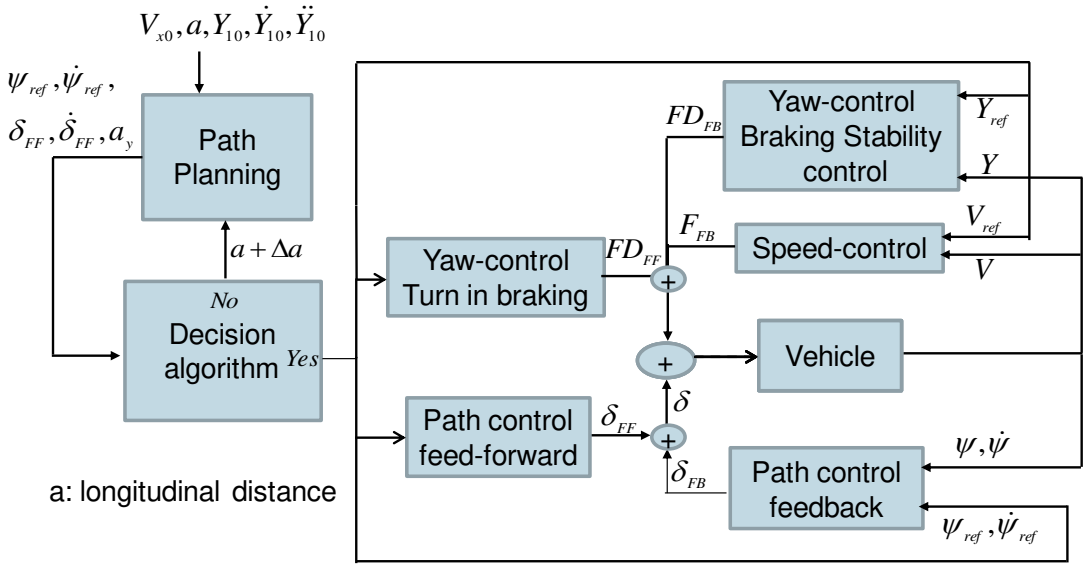

Figure 4.7 Schematic sketch of path and speed control system.

4.7 Performance evaluation

In order to evaluate the performance of the path controller, some parameters are defined as performance criteria. These parameters are defined as follow.

Path error which shows the performance of the path controller is defined as

$$e = Y_{ref} - Y \tag{4.17}$$

where the Y is the actual position of the vehicle, Y_{ref} is the desired (reference) position.

Heading angle error is defined as

$$\varepsilon = \psi_{ref} - \psi \tag{4.18}$$

where ψ is the actual heading angle of the vehicle, ψ_{ref} is the desired (reference) heading angle.

The required amount of the torque on the wheel (T) in order to perform the manoeuvre and also the rate of change in this torque ($\dot{T}$) are also taken into consideration. These parameters are basically the requirements for the steering motor and therefore are limited by the motor limitations in torque generation as well as the torque rate.

The lateral jerk i is defined as the derivative of lateral acceleration $\dot{a}_y$.

Safety margin for the distance between the host and target vehicle is defined as the minimum allowed distance between the vehicles during the manoeuvre.

Target value can be set for some parameters as follow.

Due to roll over limit, the target value for maximum lateral acceleration is set to 3.6 m/s^2 and due to the driver interaction and comfort, the maximum torque on the wheels are set to 1150Nm.

By taking into account the driver interaction and safety on one hand and the actuator limitations on the other hand the target value for maximum handwheel angle and angular speed is set to 600 deg and 500deg/s respectively.

These target values may be refined later by collecting more information about the actuator and also receiving more data from SP3 in the field of driver interaction.

5 Rear-End Collision Avoidance (RECA) - Single lane change

5.1 Optimal control results for various actuator configurations

The optimal control results are provided in this part for different actuator configurations using the simplified truck model introduced in Section 3.1.

Investigations are made to find out the advantages and disadvantages of various actuator solutions for variants of manoeuvre specifications e.g. initial speed of the collision avoidance manoeuvre and also benchmark the path stability controller.

The objective is to find F_y and F_x over [0, T] to minimize the following function:

$$J = X(T) + w\int_0^T (F_y^2 + F_x^2)\,dt \tag{5.1}$$

The particle model is also subjected to the equations of motion, friction circle as well as the lateral acceleration constraint. Maximum allowed lateral acceleration to avoid rollover risk is $a_{y,max} = 3.6\ \mathrm{m/s\hat{}2}$ for all configurations.

Initial and final condition is defined as follow:

$$X_0 = 0, Y_0 = 0, V_{x0} = 80\ \text{km/h}, V_{y0} = 0 \tag{5.2}$$

$$Y_T = 3m, V_{yT} = 0. \tag{5.3}$$

Note that the delays due to tire relaxation lengths are neglected i.e. it is assumed that the force generation is instantaneous on the wheels ($\sigma_{x,y} = 0$). The problem is solved using the software PROPT [9] with 50 nodes and the weighting factor $w = 5\mathrm{E} - 4$.

The following three different actuator configurations are studied:

- Using steering actuator for avoiding the collision

Two different cases are considered for steering actuator, for the first case, the rollover limit is the active constraints. This case is representing the high friction surfaces ($\max(a_y) = 3.6\frac{\mathrm{m}}{\mathrm{s}^2}, \mu > 0.37$). Second case is representing the low friction surface where the friction of the road is not enough for reaching the rollover limit ($max(a_y) < 3.6\frac{\mathrm{m}}{\mathrm{s}^2}, \mu < 0.37$). The Braking force is set to zero in this configuration ($F_x^D = 0$).

- Using braking actuator for avoiding the collision

Two different cases for different road conditions are considered for braking manoeuvre. Note that the Steering force is set to zero in this configuration ($F_y^D = 0$).

- Using integrated steering-braking actuator for avoiding the collision

Two different cases with different braking force and the same steering force mentioned above is considered for this case.

Figure 5.1 shows the required longitudinal distance, a^*, to perform the rear-end collision avoidance manoeuvre versus the initial velocity of the truck for various actuator configurations. The performance of these configurations is measured by the amount of required longitudinal distance for each velocity. Therefore the configuration which requires less longitudinal displacement is considered to be more beneficial for that speed. Note that the lateral displacement is only made in presence of the steering actuator. In pure braking actuator configuration simulation the lateral displacement is set to zero.

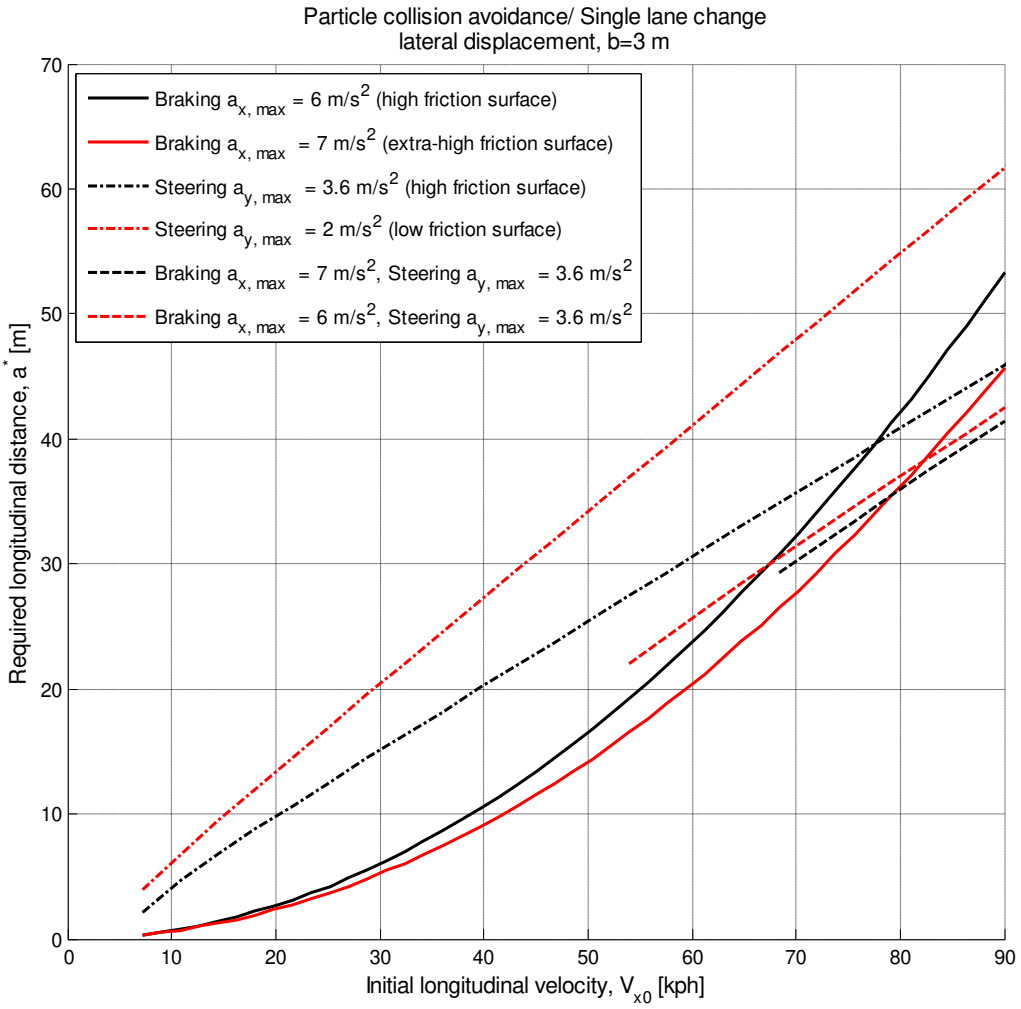

Figure 5.1 Required longitudinal distance versus initial longitudinal velocity.

These results show the break point velocity where the braking actuator configuration is not anymore the best option for avoiding the rear-end collision. Considering the curve for steering actuator configuration on high friction road with maximum longitudinal deceleration of $a_{x,max} = 6\ \mathrm{m/s^2}$, it is observed that steering becomes better than braking at 78 km/h. It is also shown in Figure 5.1, that the integrated steering-braking actuator configuration moves this point down to 68 km/h. This means that the integrated steering-braking actuator configuration gives a wider velocity range where the performance is better than pure braking. Actually, the brake point velocity for pure steering occurs at a very high velocity for a truck which results in a quite narrow velocity window. Therefore the conclusions can be made that the

integrated steering-braking actuator configuration has the potential to improve the performance of the rear-end collision avoidance manoeuvre in wide range of velocities compared to pure braking. It also covers lower velocities compared to pure steering. As expected for pure steering results, the manoeuvre on high friction surface requires less longitudinal distance since the tires are operating on the rollover limit and the required longitudinal distance increases almost linearly with the initial longitudinal velocity. Using pure braking, the results show that for different braking decelerations the gain in performance is small for low velocities but increases significantly with velocity. Therefore, it can be concluded that the effect of harsh braking is significant for high speeds.

5.2 Optimal control sensitivity study

The objective of optimal control sensitivity study is to investigate the effect of change in key parameters on the results of the rear end collision avoidance. The goal of study in each case is explained in details. Simplified truck model introduced in Section 3.1 is used for all these cases.

Lateral displacement

Optimal control problem is solved for a particle model to investigate the sensitivity of required longitudinal distance with respect to lateral distance.

The lateral distance in RECA manoeuvre is one of the main parameters. Larger longitudinal distance provides more opportunity to prevent the collision with mild manoeuvres while large lateral displacement causes more lateral acceleration, steering angle and steering angle rate and therefore a more aggressive manoeuvre. The driver comfort is also affected by harsh manoeuvre. This study shows how much can be gained by decreasing the lateral distance in the manoeuvre for example if the car in front is positioned with an offset regarding to the reference vehicle or if the vehicle is passing a motorcycle. As a result knowing the advantage of decreasing lateral displacement and considering the safety margin, defined in Performance evaluation, a desired lateral displacement can be decided.

Using pure steering actuator configuration, the objective is to find F_y over [0, T] to minimize the following function:

$$J = X(T) + w\int_0^T F_y^2 dt \tag{5.4}$$

The particle model is also subjected to the equations of motion, friction circle as well as the lateral acceleration constraint. Maximum allowed lateral acceleration to avoid rollover risk is 3.6 m/s^2 in this case.

Initial and final condition is defined as follow:

$$X_0 = 0, Y_0 = 0, V_{x0} = 80 \text{ km/h}, V_{y0} = 0 \tag{5.5}$$

$$Y_T = b, V_{yT} = 0, \; b \in [0.5,3] \text{ m} \tag{5.6}$$

The problem is solved using 50 nodes and weighting factor of $w = 5\text{E} - 4$.

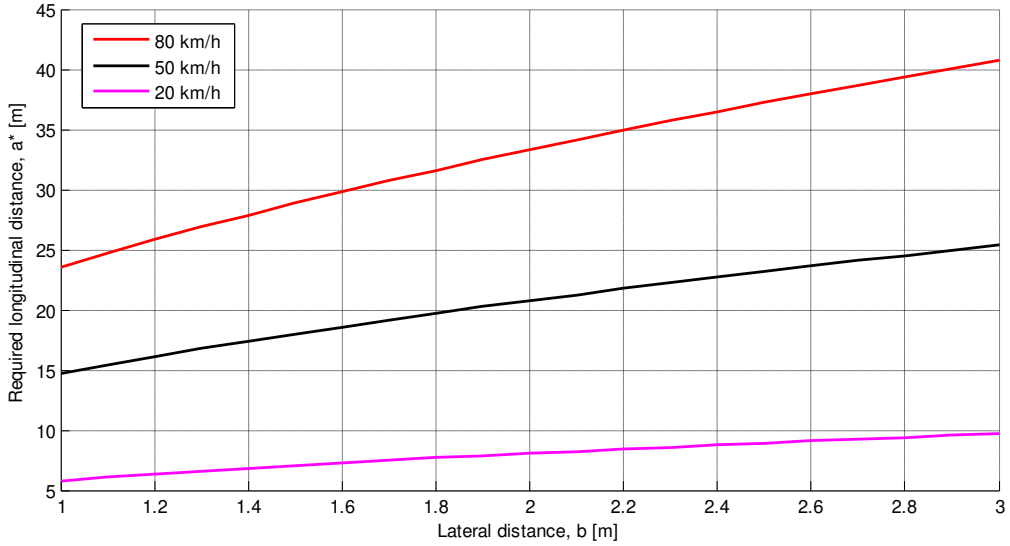

Figure 5.2 Required longitudinal distance versus lateral distance for given speed.

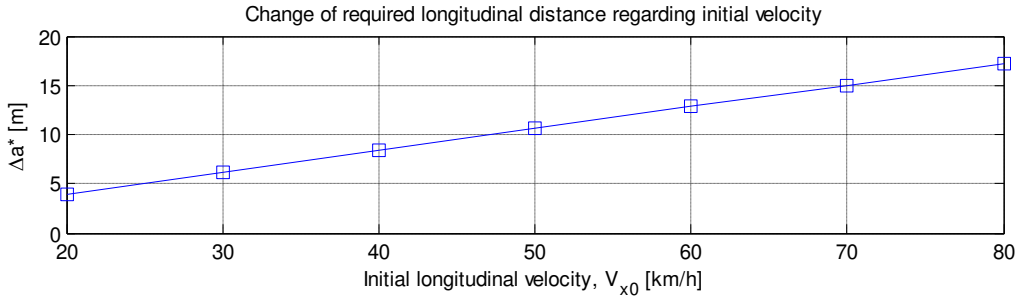

Figure 5.3 The amount of change in longitudinal distance(Δa) by reducing the lateral distance b from 3 to 1.*

As illustrated in Figure 5.2 the required longitudinal distance for the particle to avoid the obstacle by only steering is increasing almost linearly with lateral distance for all speeds.

5.2.1 Final coarse angle

Optimal control problem is solved for the particle model to investigate the sensitivity of required longitudinal distance regarding the final coarse angle which is defined as:

$$\beta_T = \tan^{-1}\left(\frac{V_{yT}}{V_{xT}}\right) \tag{5.7}$$

Final lateral velocity of the vehicle in RECA manoeuvre is a parameter which plays an important role in stabilizing and controlling the vehicle after making the manoeuvre. In general zero course angle (zero lateral velocity) in final condition is preferred. This study investigates the effect of very small course angle on efficiency of the manoeuvre. The desired result will be to find small course angles giving remarkable improvements in manoeuvre efficiency.

Using the pure steering actuator configuration, the objective is to find F_y over [0, T] to minimize the following function:

$$J = X(T) + w\int_0^T F_y^2\, dt \tag{5.8}$$

The particle model is also subjected to the equations of motion, friction circle as well as the lateral acceleration constraint. Maximum allowed lateral acceleration to avoid rollover risk is 3.6 m/s^2 in this case.

Initial and final condition is defined as follow: (The final lateral velocity of 0-14.4 km/h corresponds to coarse angle of 0-10 degree using Equation 5.7)

$$X_0 = 0,\ Y_0 = 0,\ V_{x0} = 80 \text{ km/h},\ V_{y0} = 0 \tag{5.9}$$

$$Y_T = 3,\ V_{yT} \in [0, 14.4] \text{ km/h} \tag{5.10}$$

The problem is solved using 50 nodes and weighting factor of $w = 5\text{E} - 4$.

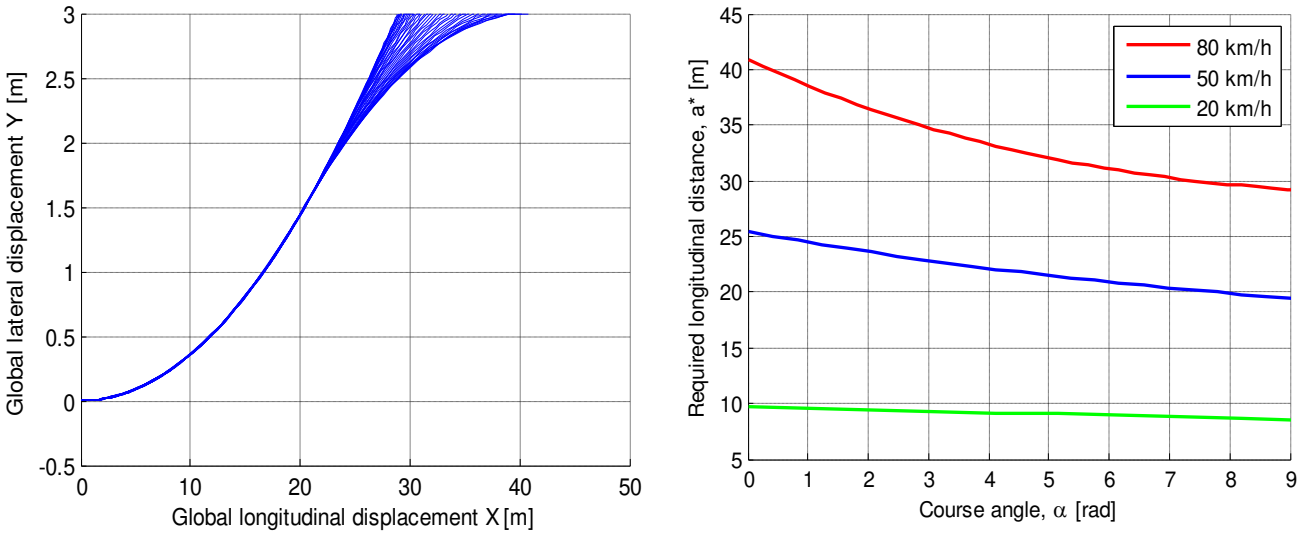

Figure 5.4 Required longitudinal distance versus final course angle.

The change in required longitudinal distance is nonlinear to course angle variation after 4 degree. And it is also observed that after 10 degree the required longitudinal distance will not change significantly with the coarse angle variation. This means that by making a small coarse angle (less than 10 degree) at the end of manoeuvre, a

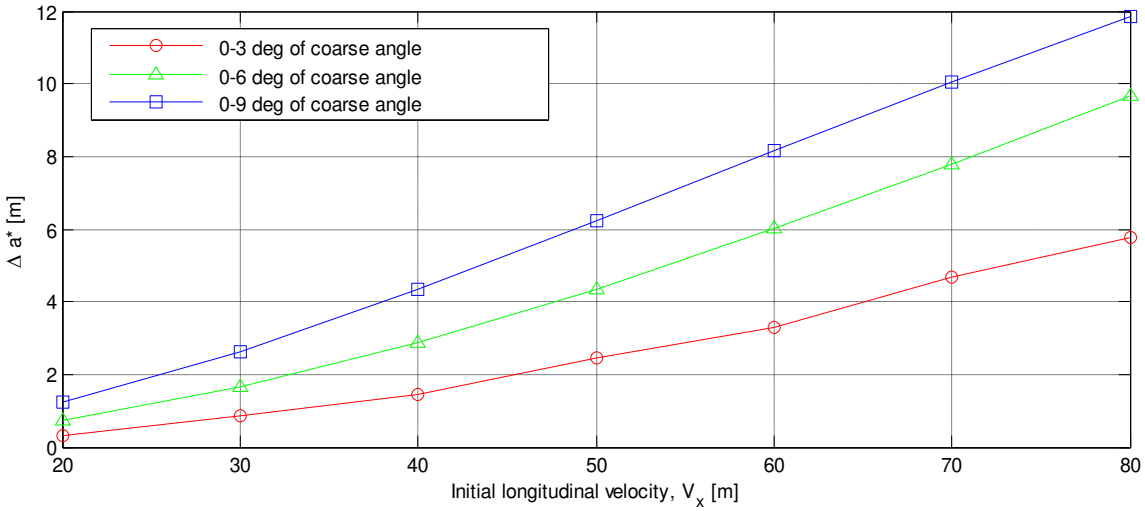

significant decrease in required longitudinal distance can be achieved.

Figure 5.5 The amount of change in longitudinal distance(Δa) by increasing the course angle.*

5.2.2 Manoeuvre severity

Optimal control problem is solved for a particle model to investigate the optimal integration of steering-braking functions with respect to the severity of the manoeuvre.

The objective of this study is to show the optimal integration of steering-braking functions in RECA considering the severity of the manoeuvre. The results of this study can be used for benchmarking the path stability control in terms of combining steering-braking function.

Using the kinematic relations, required longitudinal distance to stop the particle with the initial velocity of V_{x0} and road friction coefficient μ is calculated as

$$c = \frac{V_{x0}^2}{\mu g} \tag{5.11}$$

and the maximum lateral distance feasible with the speed of V_{x0} and friction of μ on the road is obtained from an auxiliary optimal control problem (b_{max}). The severity factor is defined as $\alpha = \frac{a}{c}$ which is the ratio of available to required longitudinal distance. Less available longitudinal distance increases the severity of manoeuvre which means lower values of alpha.

Schematic sketch of the problem is provided in Figure 3.1.

Using the integrated steering-braking actuator, the objective is to find F_y and F_x over [0, T] to minimize the following function:

$$J = V_x(T) + w\int_0^T (F_x^2 + F_y^2)dt \tag{5.12}$$

This objective function minimizes the final velocity which is one of the solutions for RECA and may be a useful method e.g. for giving the control back to driver in a lower speed which is easier to control. Moreover the forces by the actuators which is the second term of objective function can be controlled in this method e.g. performing a less aggressive manoeuvre.

The particle model is also subjected to the equations of motion, friction circle as well as the lateral acceleration constraint. Maximum allowed lateral acceleration to avoid rollover risk is 703.6 m/s^2 in this case.

Using integrated steering-braking actuator Initial and final condition is defined as follow:

$$X_0 = 0,\ Y_0 = 0,\ V_{x0} = \sqrt{\frac{\mu g a}{\alpha}},\ V_{y0} = 0 \tag{5.13}$$

$$Y_T = 0.75\ b_{\max},\ V_{yT} = 0 \tag{5.14}$$

The problem is solved using 50 nodes and weighting factor of $w = 5\mathrm{E}-4$.

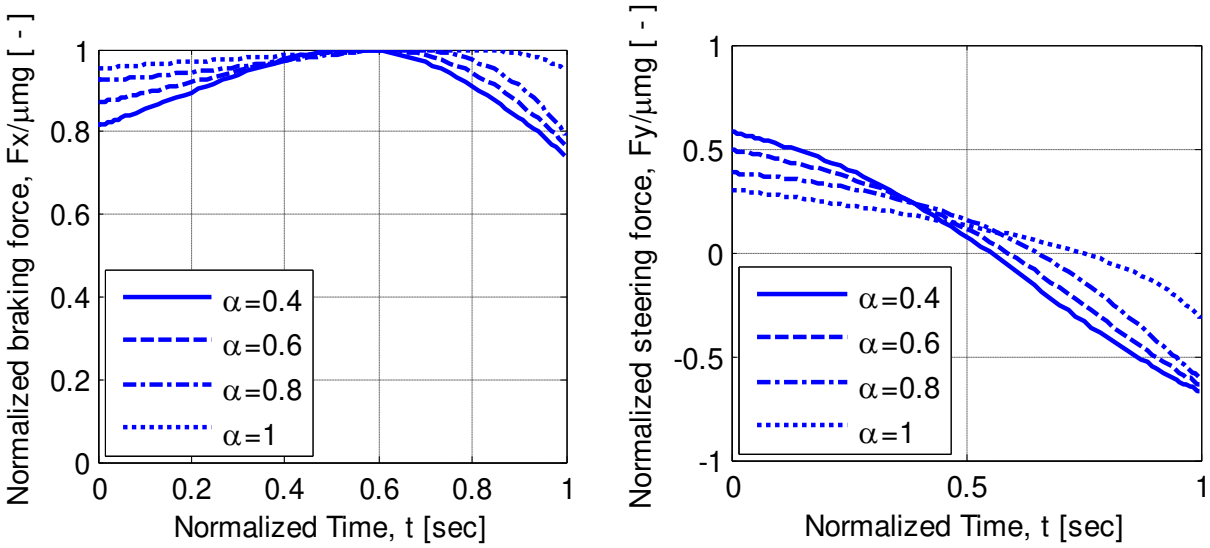

Figure 5.6 Steering-braking integration regarding the maneuver severity

It is observed from the results that for more severe manoeuvres (lower alpha values), the optimal way of integrating steering and braking is to steer more at the beginning. This is because of getting closer to last point of steer which is defined as the last point where pure steering can be applied to avoid the collision. The last point of steer can be determined from Figure 5.1 as $\alpha = 0.24$ Therefore the closer the intervention gets to this point the more steering will be needed at the beginning of the manoeuvre.

It can also be concluded from these results that if the path and speed control system is hesitating about how to combine the path and speed control due to inaccuracies, sensor problems, lack of data etc. it is the beneficial to brake at the beginning until more information is available and the severity of the manoeuvre is known. Consequently, if the manoeuvre is not severe the vehicle has not lost any opportunity by reducing the speed and going into a higher α value which means deceased manoeuvre severity. On the other hand, if the manoeuvre is severe there will be two possible scenarios. Firstly, assuming that the vehicle has not passed the last point of steer, where braking had been helpful since last point of steer is postponed by reducing the speed. Secondly, if the vehicle has passed the last point of steer, pure steering configuration will not be helpful to avoid the accident and braking or integrated steering-braking are the only available options. Consequently, it may be possible to stop the vehicle before the obstacle depending on velocity of the vehicle or avoiding the vehicle with integrated steering-braking intervention. Figure 5.1 shows when braking is better than steering. In the velocities where braking is worse there is no chance to stop the vehicle before the obstacle since the steering cannot perform the manoeuvre either. Nevertheless the accident is mitigated by braking and reducing the speed. It can be concluded braking is very often a good initial action if the required information to take the optimal action is not available.

5.2.3 Variable braking versus constant braking

This section investigates the benefit of using variable braking compared to constant braking. In constant braking the amount of braking does not change during the manoeuvre while implementing the variable braking, the braking force can freely change to obtain the optimal results.

The same problem formulation in Section 5.1 is also used here. The plots bellow shows the results of this sensitivity study.

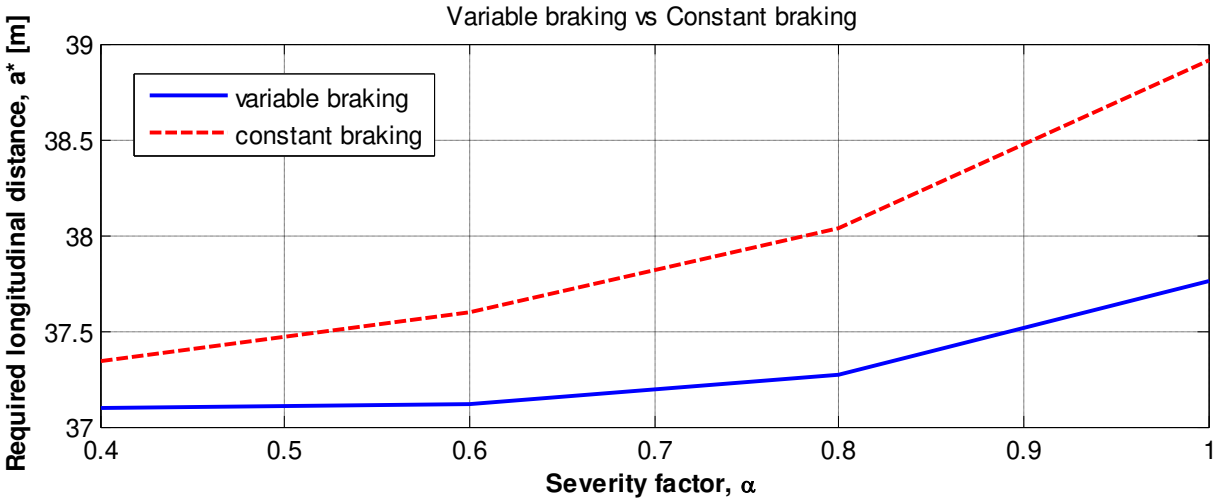

Figure 5.7 Comparing the required longitudinal distance versus the maneuver severity for constant and variable braking

This means that using variable braking, the amount of required longitudinal distance is decreased which means that the variable braking system is more efficient. It can also be observed that for more severe maneuver with higher initial speed (lower severity factor), there is small difference between constant and variable braking. However, the variable braking becomes more efficient compared to constant braking in less severe manoeuvres.

5.3 Path control simulation RECA manoeuvre

In this scenario the host vehicle is moving with the speed of V=80 km/h while the vehicle in front is standing still. The amount of lateral distance is set to 3 m and the feasible longitudinal distance will be given by path planning and decision algorithm. Figure 5.8 shows schematic sketch of the manoeuvre.

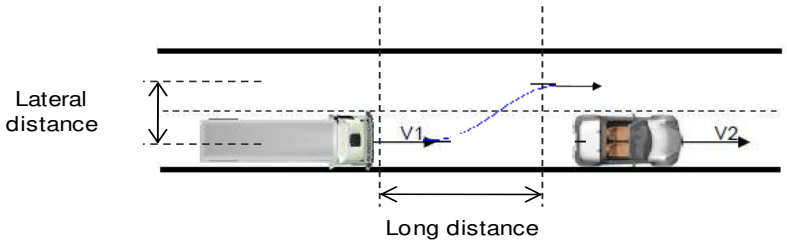

Figure 5.8 RECA simulation manoeuvre setup.

Table 5.1 shows the parameters for setting up the simulation as well as the constraints which are used in decision algorithm.

Parameters	**Values**
Input Values:	
Friction, μ	0.7
Lateral distance, b	3 m
HV initial velocity, $V1$	80 km/h
LV initial velocity, $V2$	0 km/h
Longitudinal distance, a	40 m (from path planning)
Preview time, t_p	0.4 s
Target values:	
Maximum lateral acceleration, a_x	3.6 m/s^2
Maximum hand wheel Angle, δ	600 deg
Maximum hand wheel Angle rate, ω	500 deg/s
Maximum torque on the wheel, T	1150 Nm

Table 5.1 RECA manoeuvre parameter setting.

5.4 Path control results for RECA manoeuvre

The results of the path control are divided into two parts. First the path planning results will be shown and later the path control simulation results will be illustrated. Note that pure steering actuator configuration is used for this simulation. The simulation is done on high μ surface.

5.4.1 Path planning

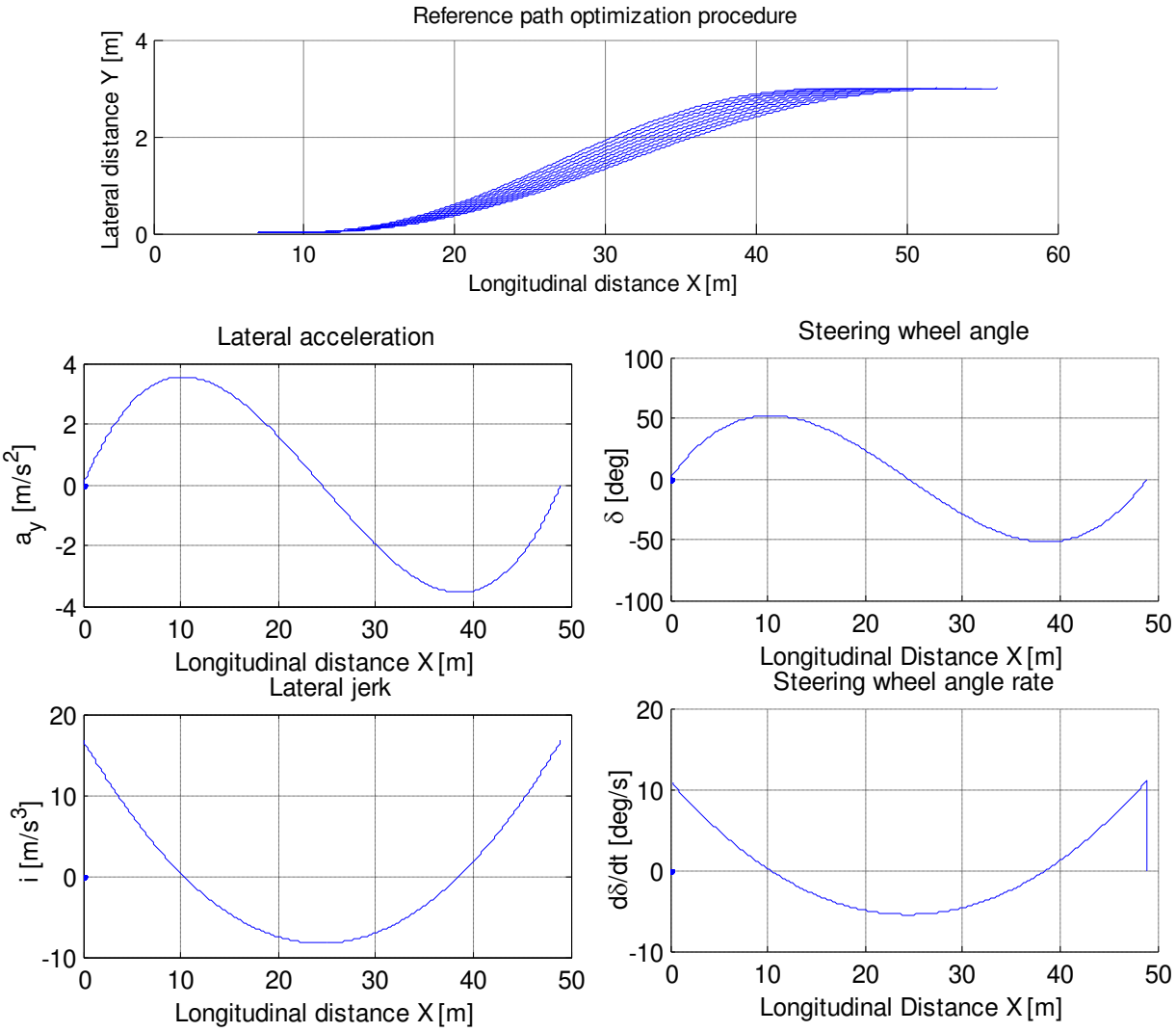

Figure 5.9 Path planning results for RECA scenario.

Following plots show the path planning outputs which are confirmed by the decision algorithm. As it can be observed, the longitudinal distance is increased in steps to meet the constraints at the decision algorithm.

It is observed in Figure 5.10 that the optimal steering angle for this manoeuvre is close to the feed-forward steering. Therefore the feed-forward steering is assumed to be good enough to be used instead of the optimal control results.

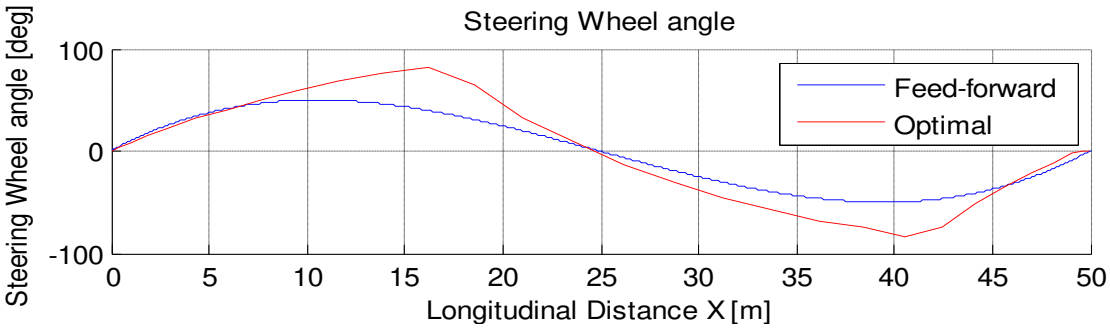

Figure 5.10 Optimal control versus feed-forward steering angle

Comparing the optimal and feed-forward steering angle which is the output of path planning algorithm in Figure 5.10, it is observed that these results are close enough to justify using the feed-forward angle as the input to the model. Therefore solving the optimal control online does not seem to be necessary in this case. These results are made for the same longitudinal and lateral distance and as expected the optimal results are obtained in higher velocity compared to path control results.

5.4.2 Simulation results

Following plots show the simulation results.

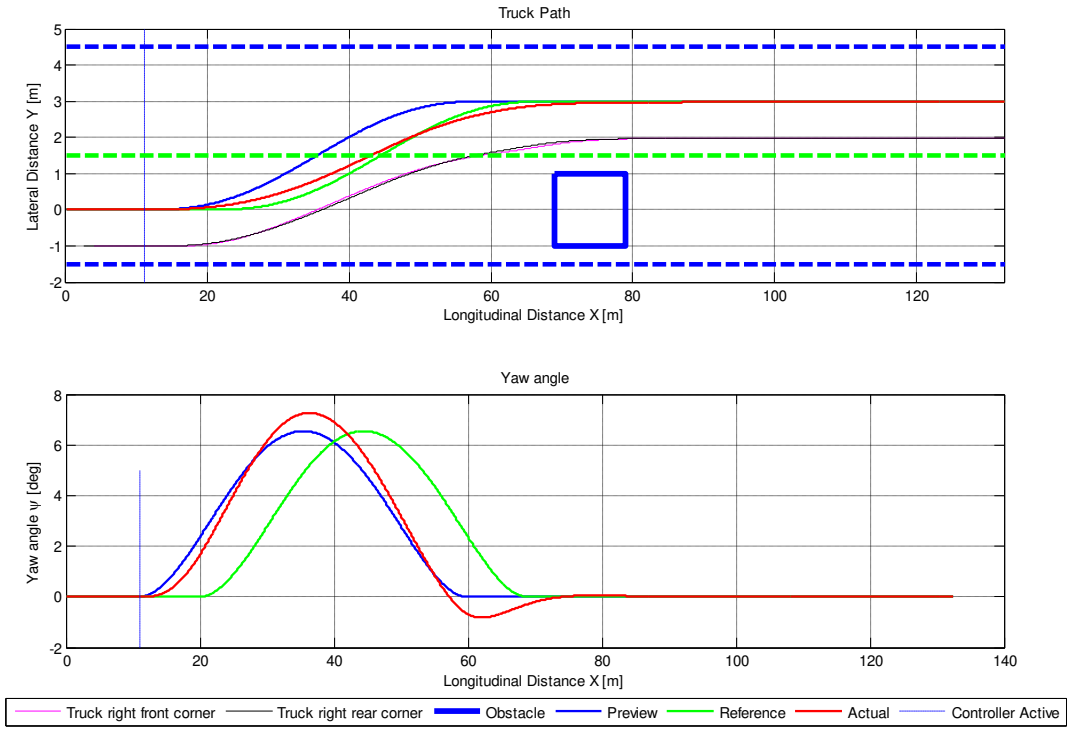

Figure 5.11 Path stability control results for RECA scenario position and heading angle

It is observed that the controller tries to cut the corners which results in lower peak for lateral acceleration in simulation results comparing with the steering angle profile provided by the path planning algorithm. The understeering behaviour of the truck is also observed considering the lines showing the position of the corners of the vehicle.

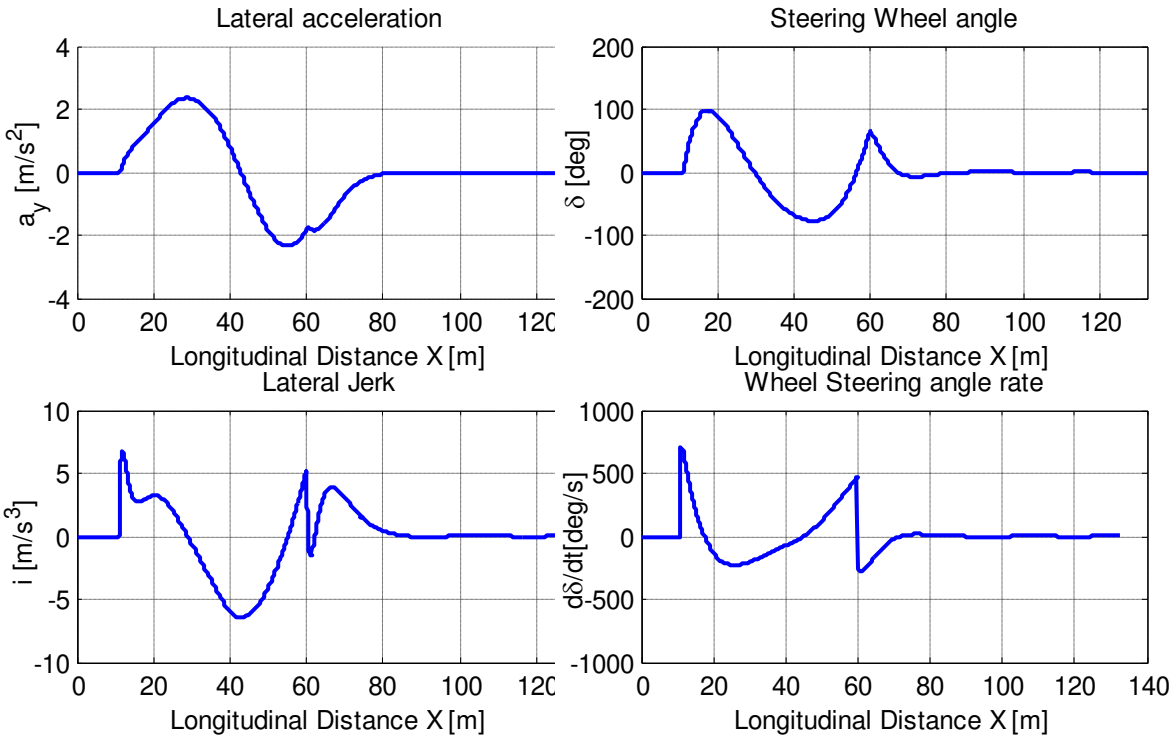

Figure 5.12 Path control results for RECA scenario steering wheel angle and torque and steering wheel rate.

As expected Counter steering is observed in presence of the feed-back control.

Tire capacity is not used significantly in this case. The reason is the low gains for the PD controller to keep the manoeuvre mild and easy to handle for the driver. It is decided that path error is not the first priority of the controller since that is avoiding the obstacle. Therefore as long as the obstacle is avoided, the gains on the controller do not need to be increased more since that will only result in harsher manoeuvre without any improvement.

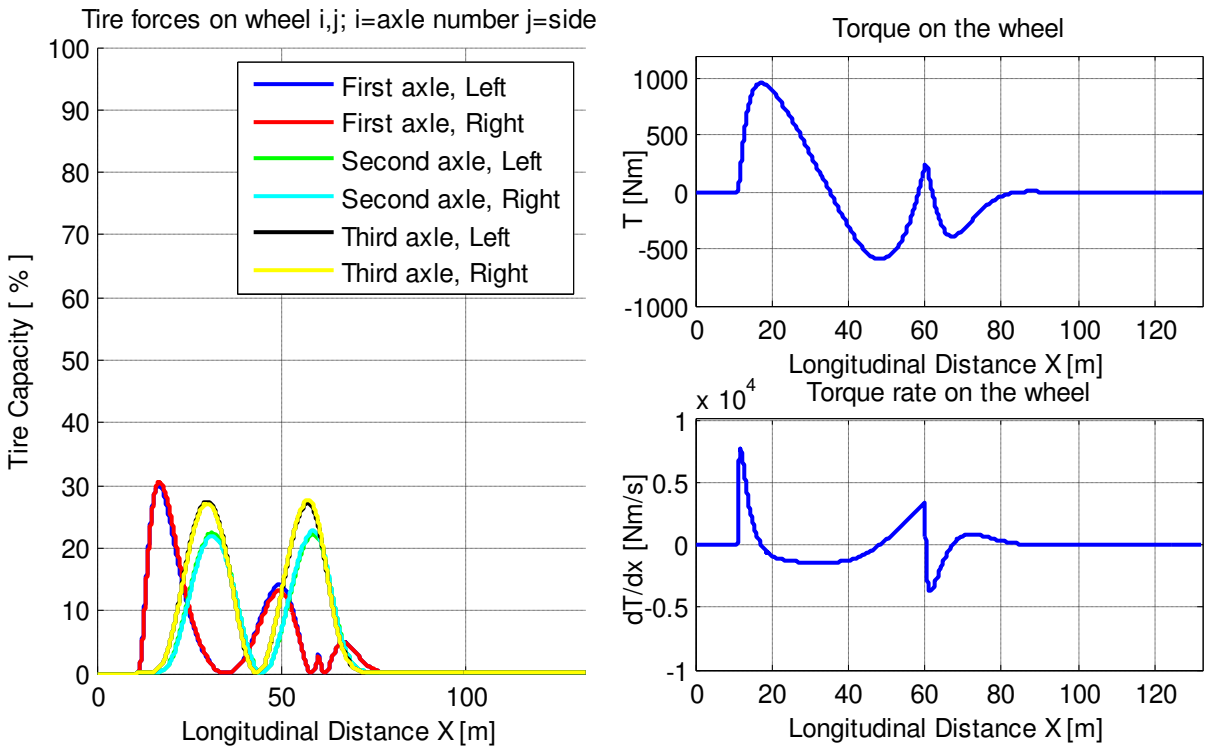

Figure 5.13 Path control results for RECA scenario - tire capacity and the torque profile

Table 5.2 shows the results of the simulation for some parameters of interest. Maximum value for each parameter, the position of the maximum value as well as the target value and the value of the parameter at the obstacle is mentioned bellow.

	Path error, e[m]	Heading angle error, ϵ[deg]	Handwheel angle, δ[deg]	Handwheel angle rate, $\dot{\delta}$[deg/s]	Lateral acceleration, ay[m/s^2]	Lateral jerk, i[m/s^3]	Wheel Torque T[N.m]	Wheel Torque rate $\dot{T}$[Nm/s]
max	0.28	3.55	98.49	714.18	2.35	6.81	958.55	7622.20
@distance [m]	33.45	55.95	17.57	11.02	28.92	11.94	17.37	11.91
desired	0.10	0.01	572.95	2800.00	3.60	0.00	1150.00	0.00
@obstacle	0.09	0.28	0.07	0.76	0.91	3.48	366.90	0.00

Table 5.2 RECA path control simulation results.

5.5 Path and speed control for RECA manoeuvre

This section mainly deals with the integrated steering-braking actuator in collision avoidance manoeuvre. The optimal control results are used in order to improve the understanding of a proper integration of steering and braking actuators.

The controller is turned to a path-speed controller in this case where a proportional controller is active on the speed in this case. The speed profile is also given in advance from the path planning algorithm. Note that integrated steering-braking control is used in these simulations.

5.5.1 Path control results

The results of simulation for steering-braking integration are as follow. Note that the simulation is done on high μ surface.

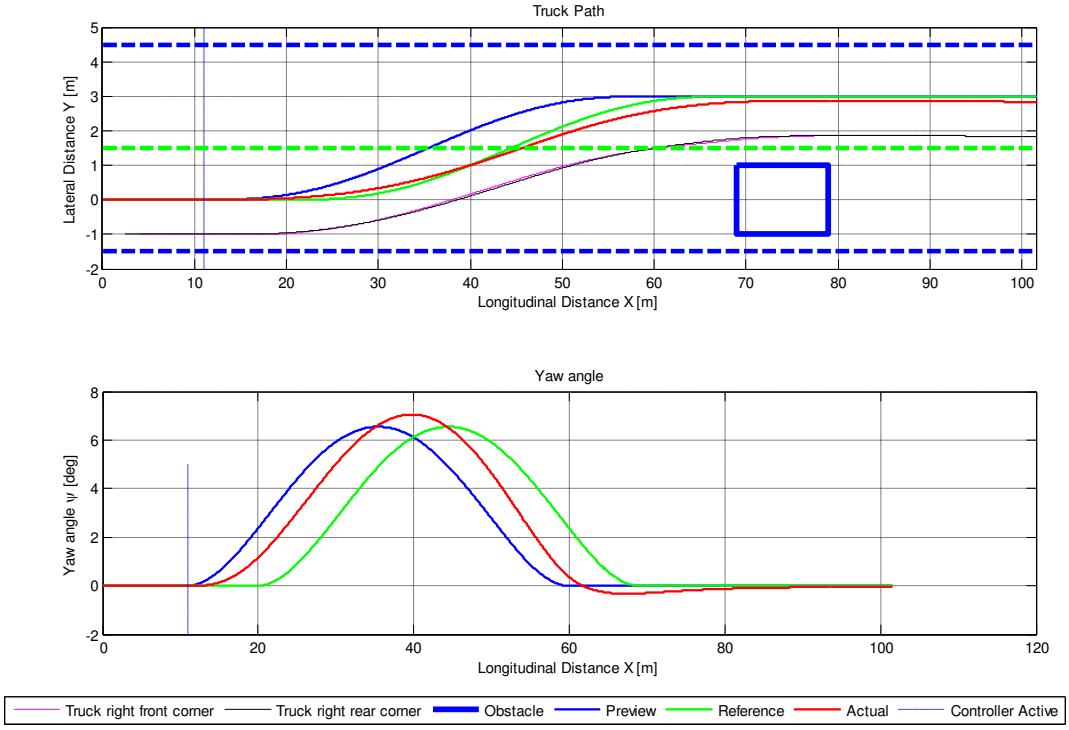

Figure 5.14 Path and heading angle profile for integrated steering braking actuator for RECA scenario

It can be observed that the heading angle profile is followed more accurately using the braking. The reason for this behaviour can be that the brake force is distributes more force on front wheel therefore, the front cornering stiffness decreases more than on other axles. As a result, the vehicle becomes more understeered and can easier follow the path.

It is also observed that there is more offset at the end of the manoeuvre using braking. This is due to the decrease in cornering stiffness and therefore the loss in lateral force.

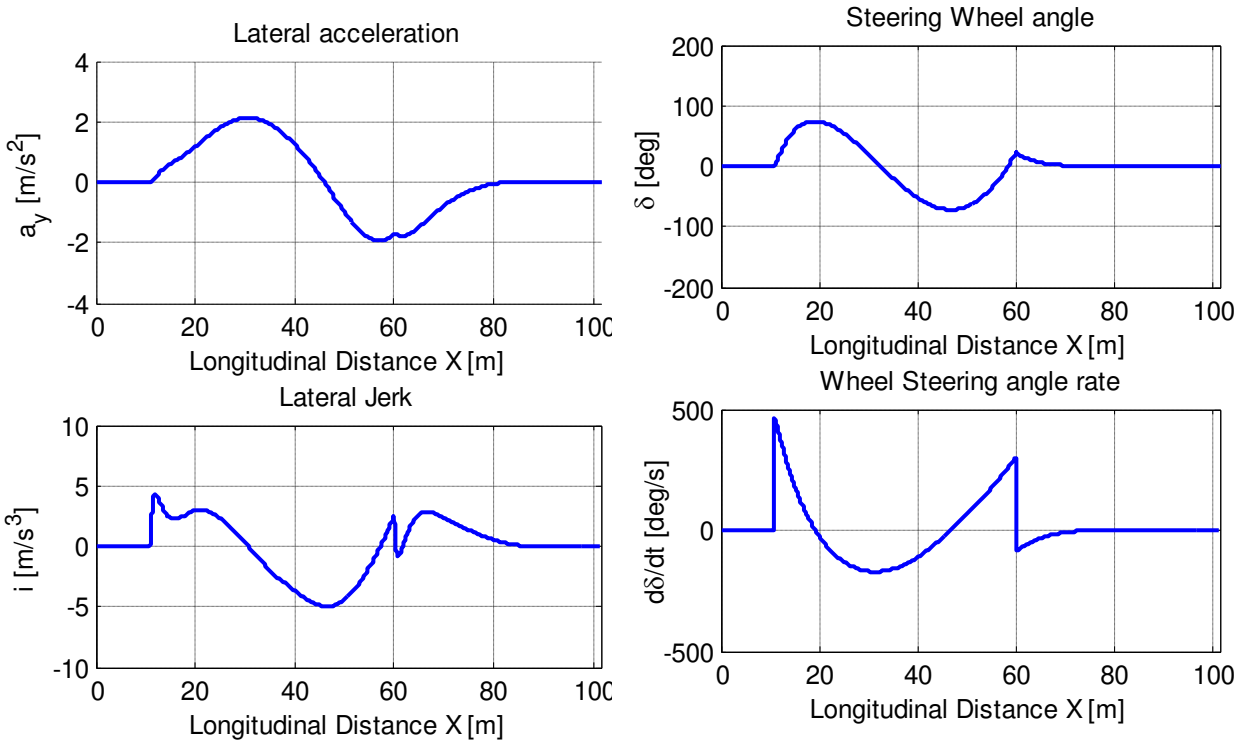

Figure 5.15 Path stability control results for integrated steering-braking actuatorconfigurations for RECA. lateral acceleration, steering wheel angle and the torque and steering angle rate.

Comparing these results with pure steering, It can be observed that the steering wheel angle and also steering wheel rate is decreased. A decrease in lateral acceleration as well as the torque on the wheel and their time derivatives is also observed.

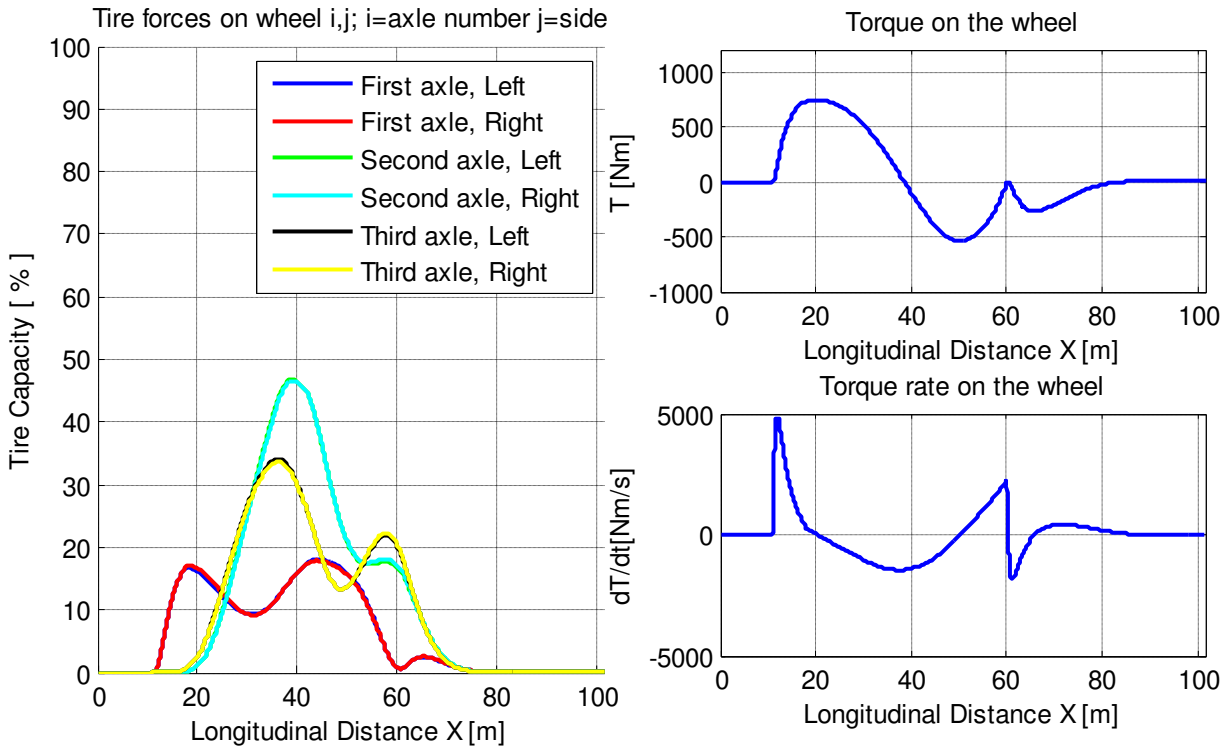

Figure 5.16 Path control results for integrated steering braking actuator for Rear End collision avoidance scenario - tire capacity and the torque profile on the wheel.

It is seen that more of tire capacity is used using the braking which is expected compared with the only steering case.

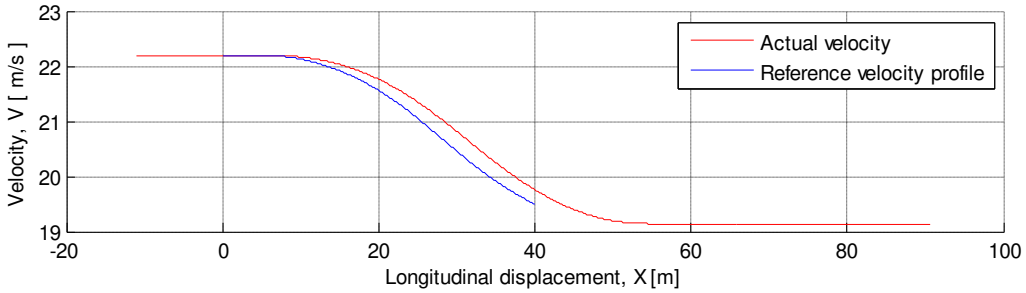

Figure 5.17 Path control results for integrated steering braking actuator for RECA scenario. Speed profile

Investigating the results of the path control sensitivity study, it is observed that the results of the integrated steering-braking actuator configuration are not significantly better than the pure steering. Comparing these results with optimal control results that showed a reduction in required longitudinal distance, it can be concluded that the sophisticated integration of steering braking actuators in optimal control solution cannot be easily implemented in the path controller.

5.6 Path and yaw control for RECA manoeuvre

The intention of implementing the turn in braking actuator configuration is to increase the manoeuvrability of the truck by making it respond faster to steering demand. This system can be basically applied as assistance for steering actuator. The other usage of the differential braking is to assist the steering for stabilizing the vehicle. The algorithm of differential braking implemented in this study is described in details in Section 4.4. The simulation is done on high μ surface.

Note that the turn in braking actuator configuration is combined with pure steering configuration in this simulation.

5.6.1 Turn in braking

To investigate the performance of the initial differential braking, the simulation is done for the case with and without the initial differential braking (turn in braking). The problem with this approach is that when the shorter preview time is applied, the over shoot after the lane change is not avoidable if the path is followed with a high accuracy. This phenomenon, which is due to truck yaw dynamics will be discussed later in this part. The steering control is the same for the previous cases with only steering. The following plots are the results of these simulations.

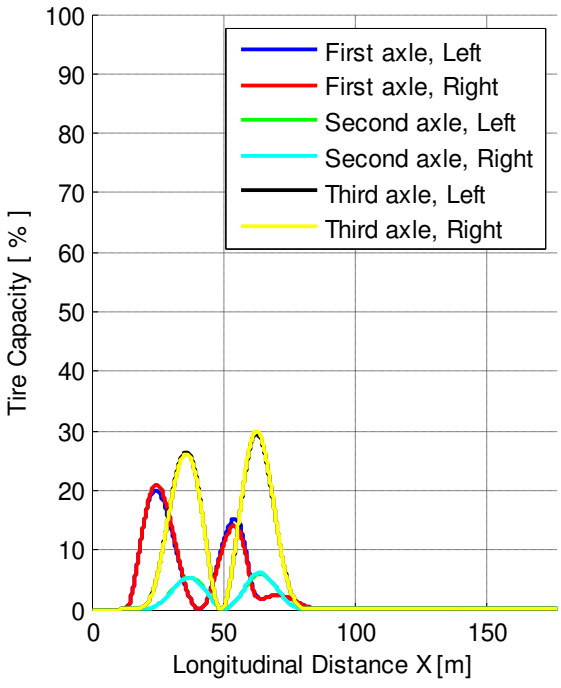

Figure 5.18 Tire force capacity witout turn in braking.

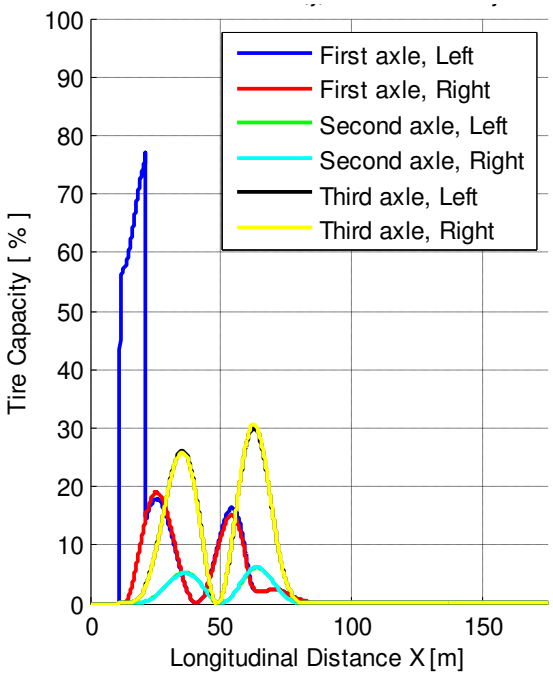

Figure 5.19 Tire force capacity with turn in braking.

The shape of the first axle left wheel force curve shows a superposition of the steering and differential braking at the beginning of the manoeuvre. It is observed that the curve almost goes back to pure steering when the differential braking ends. Figure 5.20 shows that the differential braking makes the vehicle faster in following the

heading angle profile. On the other hand both overshoot and final position offset is increased.

The reason for the offset is that the feedback controller is correcting the inputs based on the heading angle and heading angle rate. Therefore if a change in condition happens e.g. losing friction on the road, the controller is not able of taking the vehicle to the right position. Furthermore it can be stated that the more precise the vehicle follows the path in short preview times or higher speeds the more final overshoot will be expected.

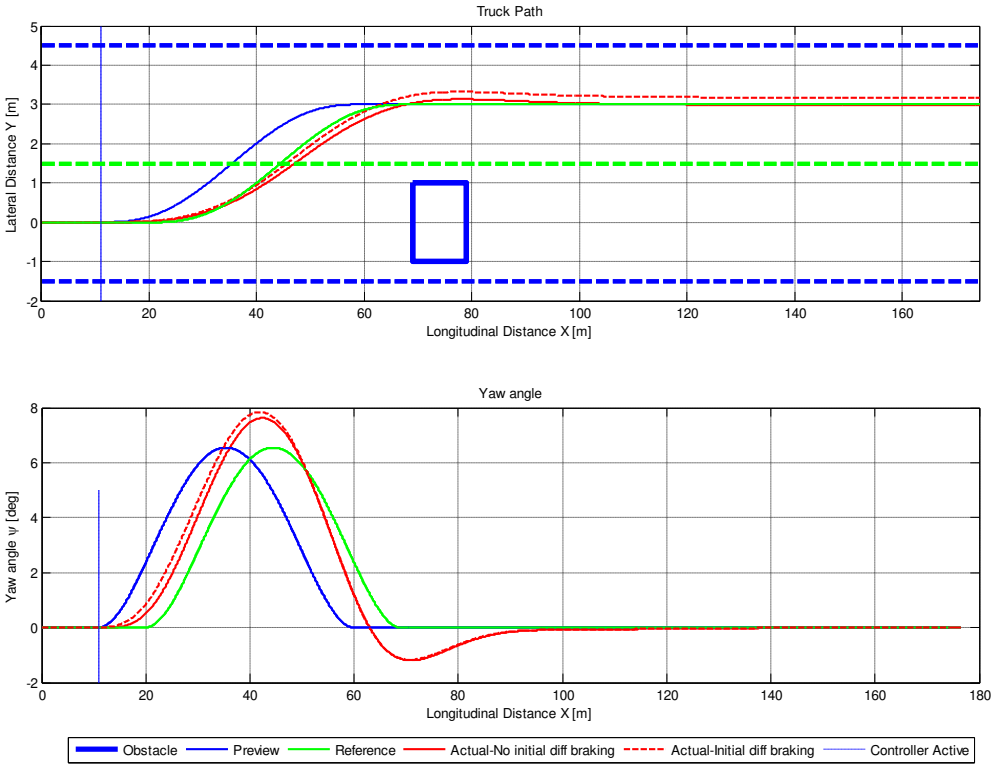

Figure 5.20 Path and heading angle profile for the cases with and without the turn in braking respectively.

5.6.2 Braking stability control

In order to compensate the final position offset, caused by Turn in braking, the final differential braking (brake stability control) is implemented as the feedback control operating on the position error for compensating any kind of inaccuracy in estimating the friction or even the change in manoeuvre condition. This method is applied to the previous case with the offset to investigate the performance of the system. Note that the braking stability actuator configuration is combined with the pure steering configuration for this simulation.

The results are as follow:

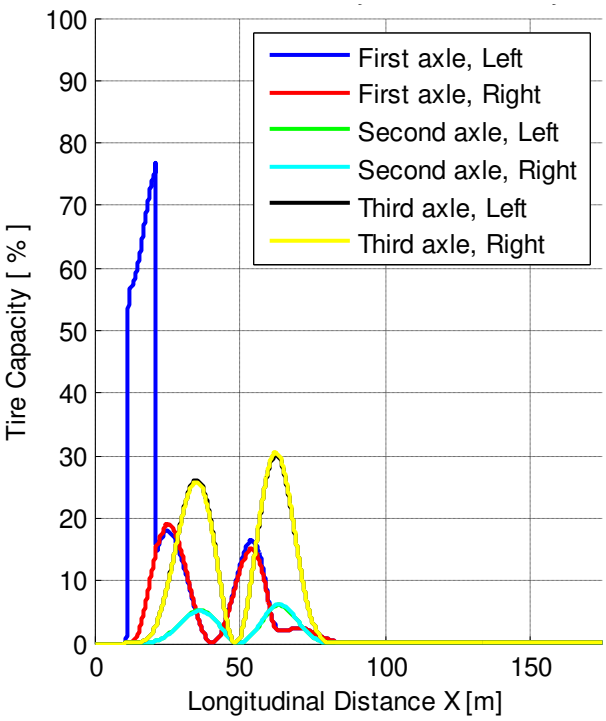

Figure 5.21 Tire force capacity with turn in braking.

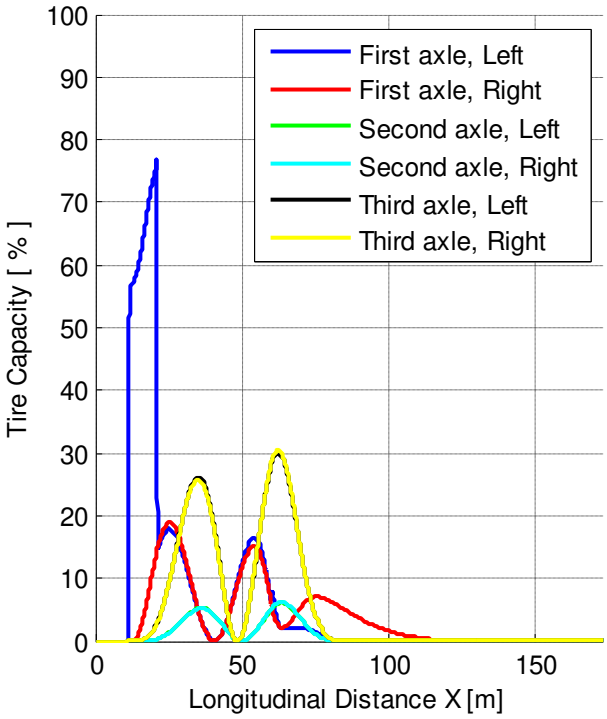

Figure 5.22 Tire force capacity with turn in braking and brake stability control.

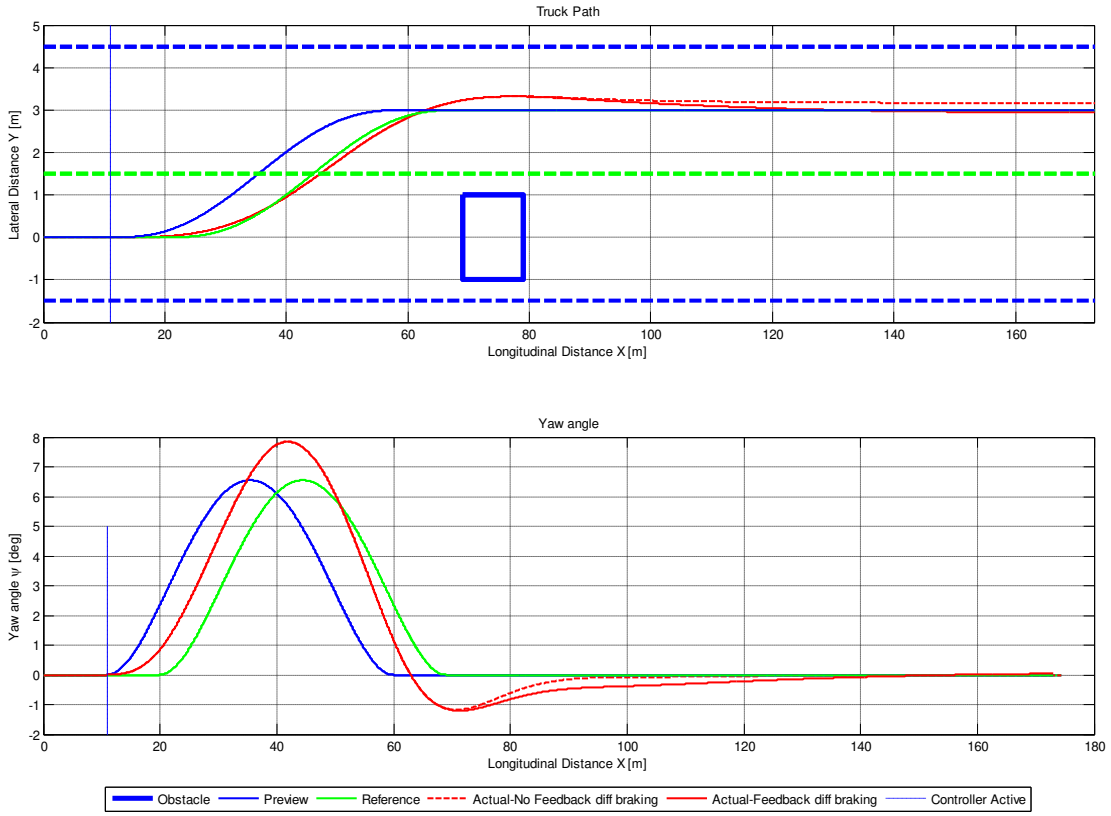

Figure 5.23 Path and heading angle profile for the cases with and without the brake stability control respectively.

The advantage with this method is that the steering wheel oscillation at the end of the manoeuvre will be decreased. This can be counted as a big improvement for driver interaction point of view.

Therefore as the final configuration for differential braking application, the differential braking is used at beginning of the manoeuvre as the feed-forward input and at the end of manoeuvre as the feedback for compensating the offset. The rest of the manoeuvre is left for the steering actuator.

It should be also stated here that a very light braking before the manoeuvre starts should be applied to the vehicle. There are different advantages with this action.

- Getting the proper information about the friction on the road
- Keeping the brakes as fast as possible in order to having less delay while using differential braking
- Making the tire more laterally stiff and therefore getting a better steering performance at the beginning of the manoeuvre
- Pre-tensioning the seat belt
- Warning the driver

This part is not considered in the simulation.

5.7 Path control sensitivity study

Figure 5.24 shows the required longitudinal distance to perform a RECA manoeuvre with respect to the initial longitudinal velocity.

Comparing these results with Figure 5.1, it is observed that the intersection point between the braking curve with $a_x = -6$ m/s^2 and the steering curve with $a_y =$ 3.6 m/s^2 is moved to 87 km/h which means that the steering strategy becomes better than braking in even higher velocities.

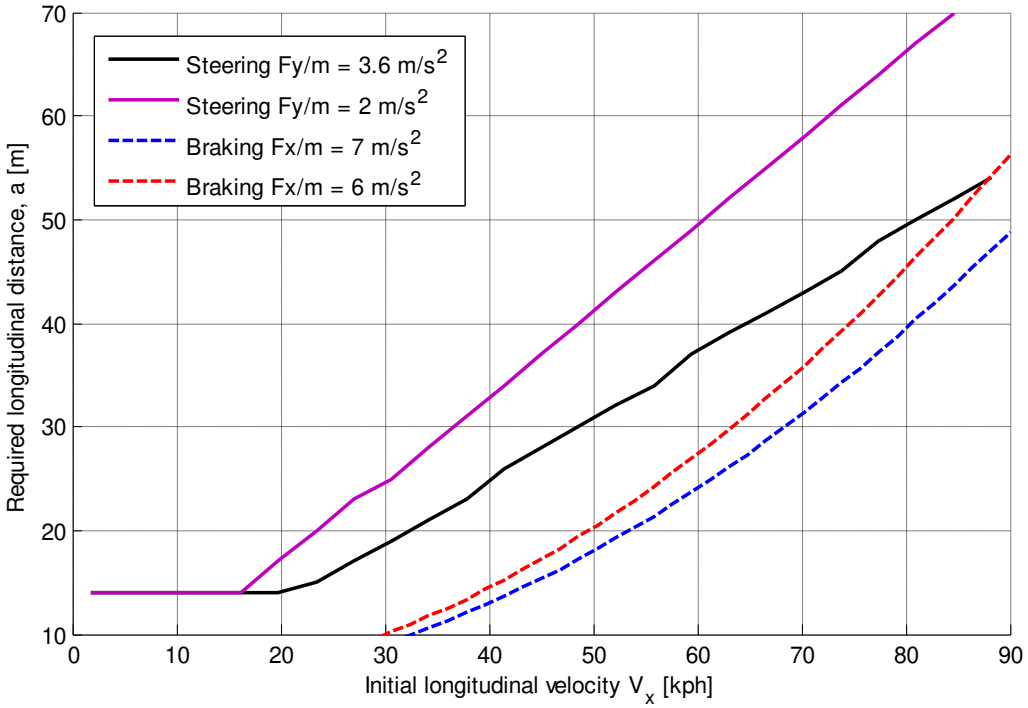

Figure 5.24 Required longitudinal distance versus initial longitudinal velocity.

5.8 Comparison of optimal and path stability control

Considering the pure steering actuator configuration, results of optimal and path control are compared for two different cases.

It can be observed in the Figure 5.25, that the optimal results are better than the path control as it is expected. However this difference is larger than expected. The reason for this is the additional constraints on the path control decision algorithm such as steering angle rate that makes the path controller results worse than the optimal control.

Moreover after 14 meter of longitudinal displacement, the path stability control simulation longitudinal distance does not decrease by the velocity. The reason for this behaviour is the constraints on steering angle and steering angle rate in path stability control decision algorithm which does not allow less longitudinal distance. Note that the delay on the force generation is set to zero for both optimal and path stability control simulation.

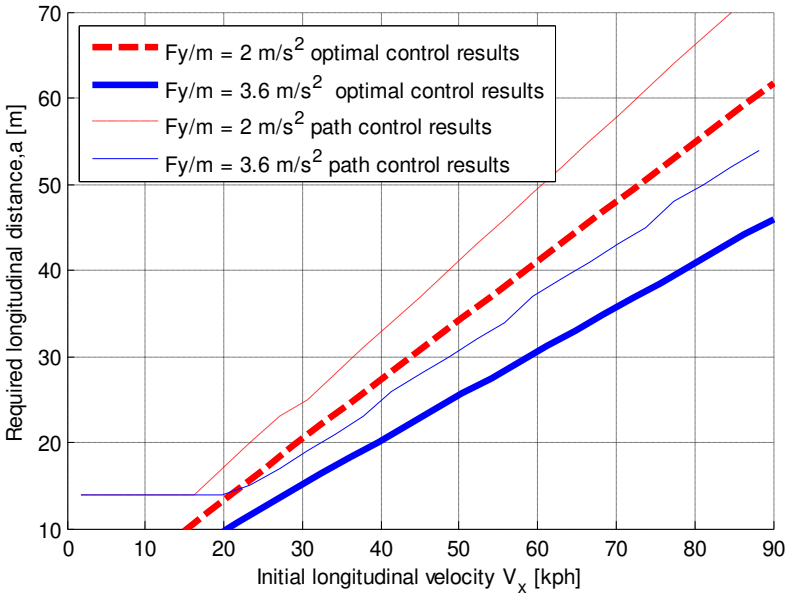

Figure 5.25 Required longitudinal distance versus initial longitudinal velocity for steering actuator configuration.

Considering the pure braking actuator configuration, results of optimal and path control are compared for two different cases. Figure 5.25 shows that the optimal control results are better than the path stability control simulation results. The difference is a bit larger than expected and this difference is due to the braking force distribution on the axles. It worth to mention that for making a logical comparison the delays on force generation is set to zero in both optimal control and path stability control simulation.

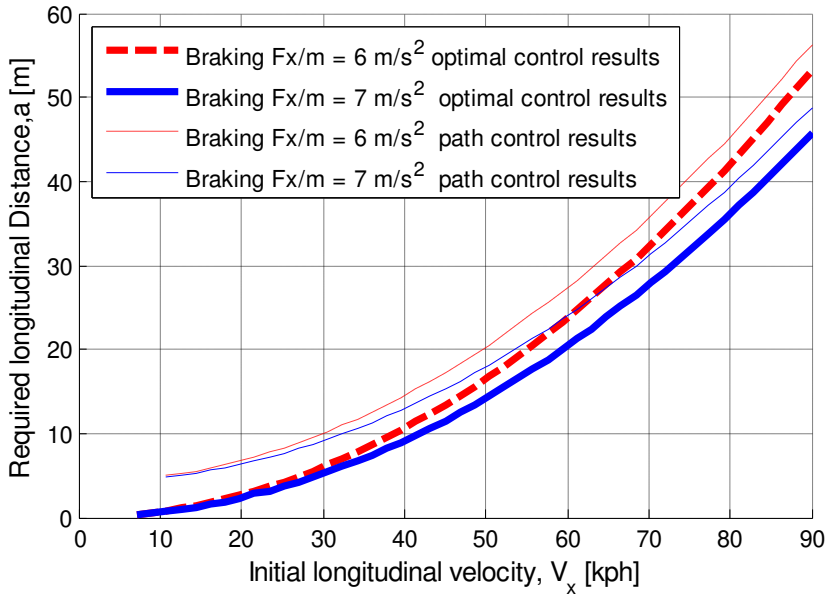

Figure 5.26 Required longitudinal distance versus initial longitudinal velocity for braking actuator configuration.

6 Run-off-road prevention (RORP)

6.1 Path control simulation RORP manoeuvre on straight road

Run-off prevention scenario is simulated in two different configurations. First configuration deals with Run-off prevention on a straight road. Second case studies the same scenario where a curved road is considered with a large radius.

The difference in these two cases is that in the first case there is a false action by the driver due to the drowsiness for instance while in second case, lack of action from driver is detected. Therefore the job of controller in first case is to correct the driver and take the vehicle back to road, while in second case the controller tries to compensate the absence of driver's action.

In this scenario the vehicle is moving longitudinally with the speed of 65 km/h. Driver applies a small steering angle. When the vehicle reaches one of the heading angle or lateral displacement limit, the controller goes active and takes the vehicle back to the road. The Driver input is modelled by a feed forward steering input to the vehicle. The feasible longitudinal distance is the result of path planning which satisfies the constraints on decision algorithm.

The limitation on heading angle and lateral displacement is as follow.

$$\psi_{max} = 5\ deg$$
$$y_{max} = 20\ cm$$

Figure 6.1 shows a schematic sketch of the simulation manoeuvre setup.

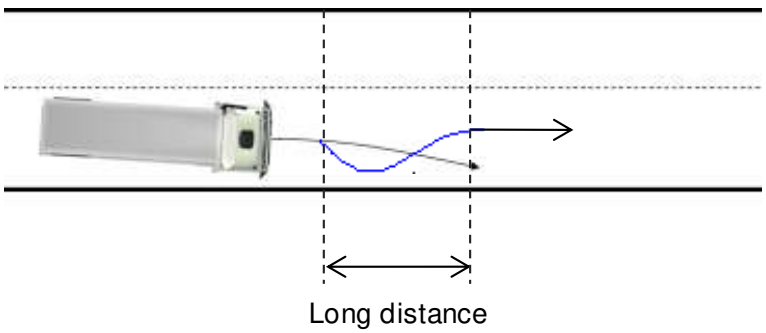

Figure 6.1 RORP simulation maneuver setup

Table 6.1 shows the parameters for setting up the simulation as well as the constraints which are active in decision algorithm.

Parameters	Values
Input Values:	
Friction, μ	0.7
HV initial velocity, V_0	65 km/h
Longitudinal distance, a	16 m (from path planning)
Preview time, t_p	0.4 s
Target values:	
Maximum lateral acceleration, a_y	3.6 m/s^2
Maximum hand wheel Angle, δ	600 deg
Maximum hand wheel angle rate, ω	500 deg/s
Maximum torque on the wheel, T	1150 Nm

Table 6.1 RORP maneuver parameter setting.

6.2 Path control results for RORP on straight road

The results of the path stability control are divided into two parts. First the path planning results will be shown and later the path stability control simulation results will be illustrated. Note that only the steering control is used in this simulation. The simulation is done on high μ surface.

6.2.1 Path planning

Following plots show the path planning outputs which are confirmed by the decision algorithm. As it can be observed, first part of the path is given by a feed forward steering angle which is not inside the controller active zone. When the vehicle reaches the limitation of either lateral displacement or heading angle, the controller becomes active. For controller active zone the longitudinal distance is increased in steps to meet the constraints at the decision algorithm.

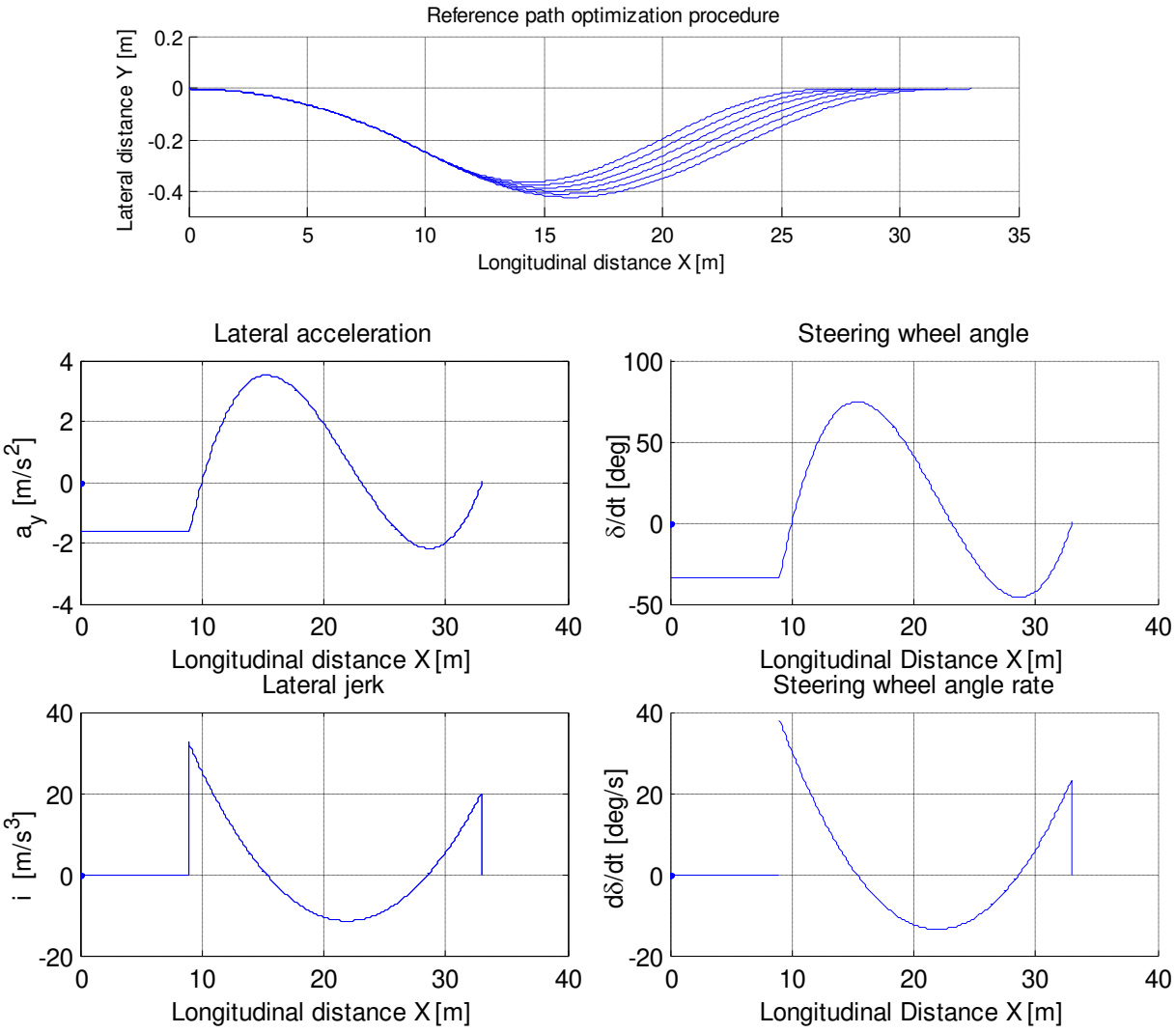

Figure 6.2 Path planning results for RORP scenario.

6.2.2 Simulation results

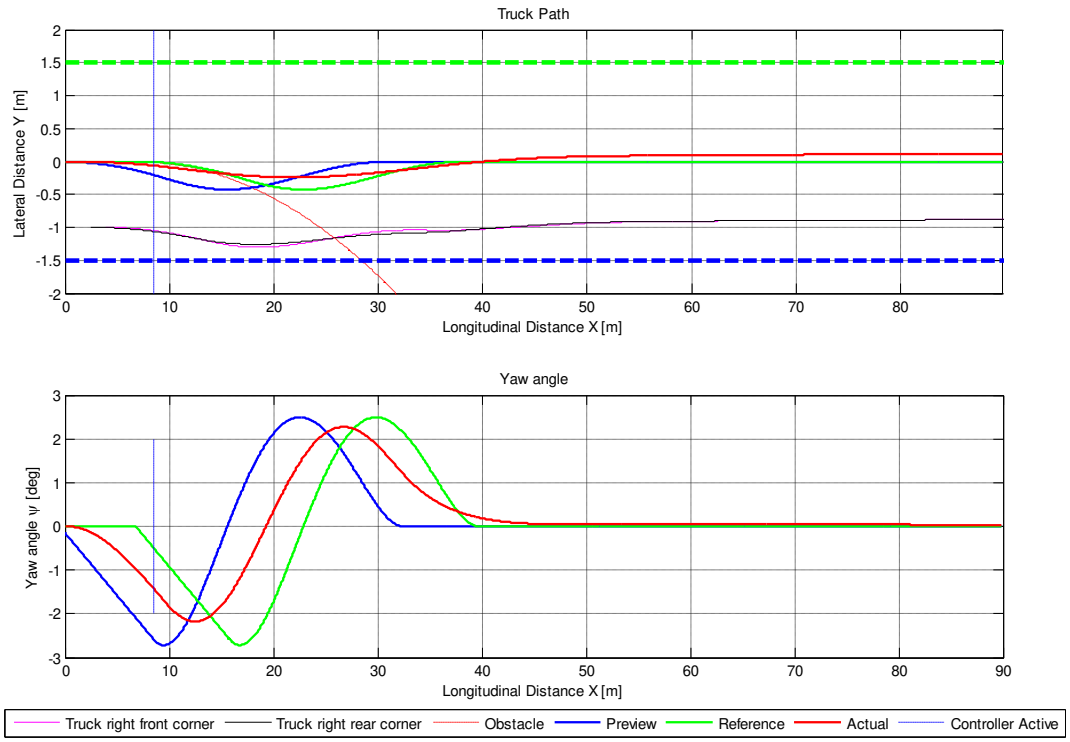

Figure 6.3 Path stability control results for RORP scenario- position and heading angle

As it is observed in plots, in absence of the controller the vehicle will follow the dashed red line

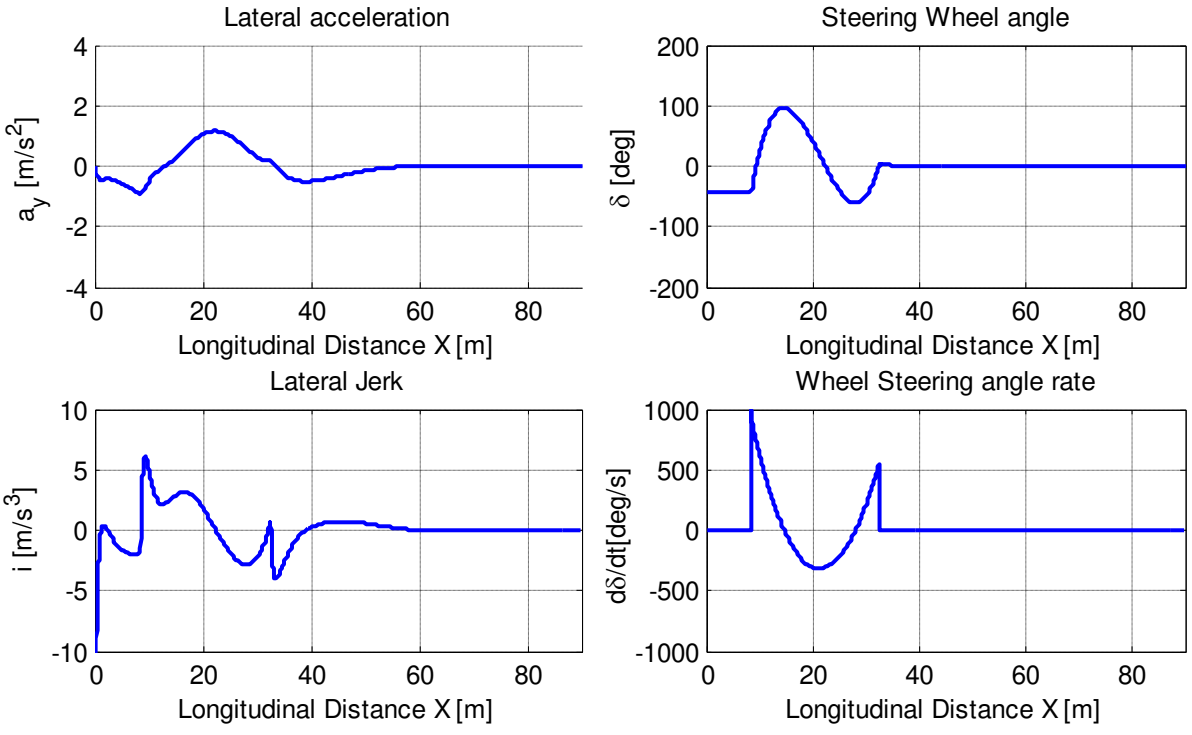

Figure 6.4 Path stability control results for RORP scenario-steering wheel angle and their time drivitives

Counter steering which is done by the feedback controller is observed. Counter steering is very small here due to small gains on the feedback control.

High peaks of steering angle rate and also the lateral jerk and torque will be filtered if applied to an actuator. Therefore the need of filtering them in the simulation was not observed.

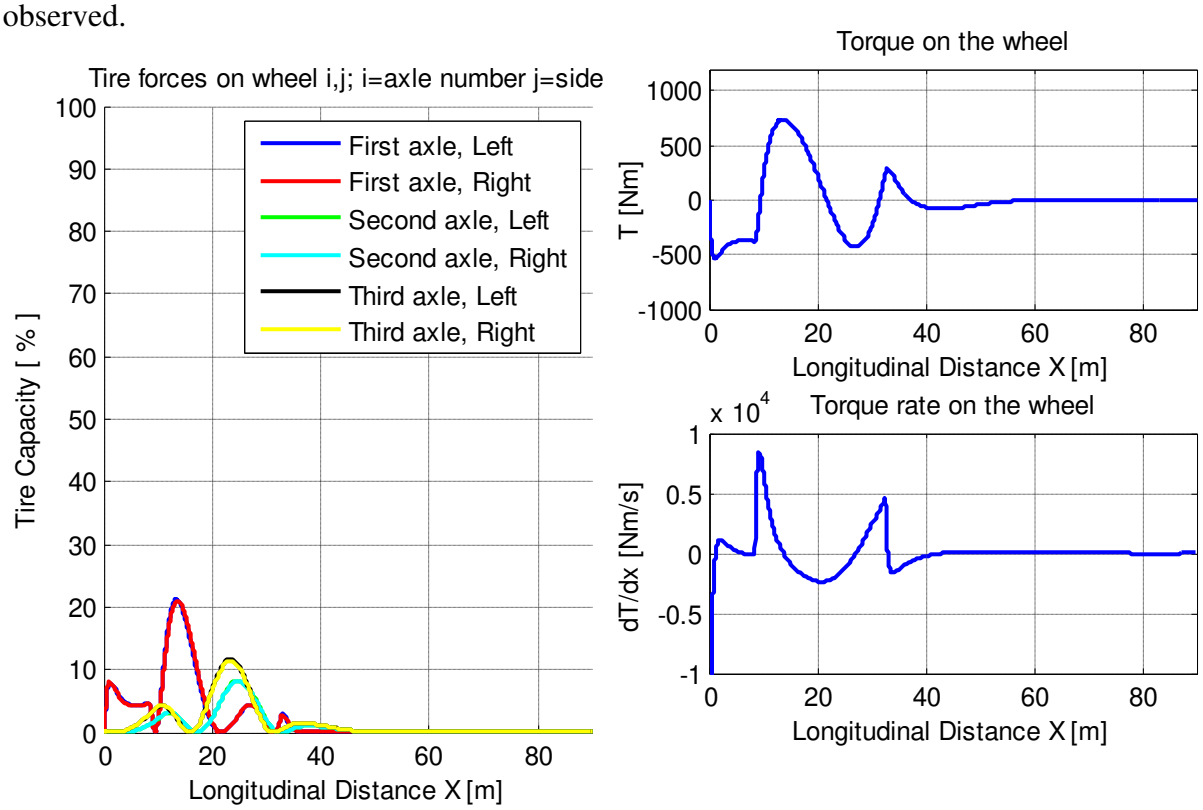

Figure 6.5 Path stability control results for RORP scenario tire capacity and the torque profile

Similar to previous scenario, the tire capacity is not used a lot in this case. The same reason can be motivated here as well. By increasing the gains on the feedback control, more of tire capacity will be used by penalizing the stability.

Table 6.2 shows the results of the simulation for some parameters of interest. Maximum value for each parameter, the position of the maximum value as well as the target value and the value of the parameter at the obstacle is mentioned bellow. The high values of steering angle rate and wheel torque rate will not be this high in implementation since they will be filtered by actuator dynamics.

	Path error, e[m]	Heading angle error, ϵ[deg]	Handwheel angle, δ[deg]	Handwheel angle rate, $\dot{\delta}$[deg/s]	Lateral acceleration, ay[m/s^2]	Lateral jerk, i[m/s^3]	Wheel Torque T[N.m]	Wheel Torque rate $\dot{T}$[Nm/s]
max	0.19	2.08	95.97	1425.94	1.16	23.07	739.81	26396.29
@distance [m]	23.19	19.58	14.66	8.50	22.36	0.00	13.76	0.00
desired	0.10	0.01	572.95	2800.00	3.60	0.00	1150.00	0.00

Table 6.2 RORP path control simulation result

6.3 Path control simulation RORP manoeuvre on curved road

In this simulation manoeuvre configuration the driver is driving with the velocity of 65 km/h on a curved road with a high radius. On the curve the driver stops steering which is needed to stay on the road. The controller becomes active and takes the vehicle back to the road when either heading angle or lateral displacement limitation is reached by the vehicle.

The limitation on heading angle and lateral displacement is as follow.

$$\psi_{max} = 5\ deg$$

$$y_{max} = 10\ cm$$

Figure 6.6 shows a schematic sketch of the simulation manoeuvre setup.

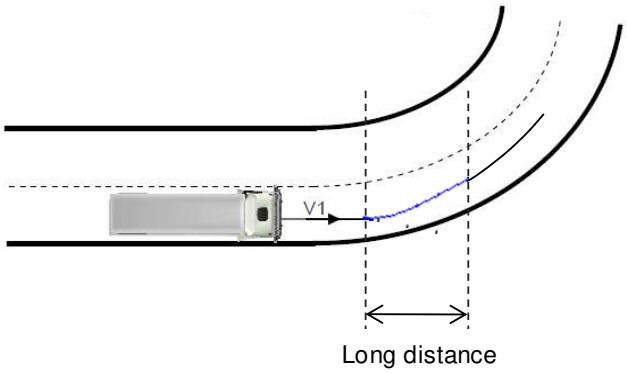

Figure 6.6 RORP simulation setup

Table 6.3 shows the parameters for setting up the simulation as well as the constraints which are active in decision algorithm.

Parameters	**Values**
Input Values:	
Friction, μ	0.7
HV initial velocity, V_0	80 km/h
Longitudinal distance, a	32 m (from path planning)
Preview distance t_p	18 m
Target values:	
Maximum lateral acceleration, a_y	3.6 m/s^2
Maximum hand wheel Angle, δ	600 deg
Maximum hand wheel angle velocity ω	500 deg/s
Maximum torque on the wheel T	1150 Nm

Table 6.3 RORP maneuver parameter setting.

6.1 Path control results for RORP on curved road

The results of the path stability control are divided into two parts. First the path planning results will be shown and later the path stability control simulation results will be illustrated. Note that only the steering control is used in this simulation. The simulation is done on high μ surface.

6.1.1 Path planning

Following plots show the path planning outputs which are confirmed by the decision algorithm. When the vehicle reaches the limitation of either lateral displacement or heading angle, the controller becomes active. For controller active zone the longitudinal distance is increased in steps to meet the constraints at the decision algorithm. Note that only the steering control is used in this simulation. The simulation is done on high μ surface.

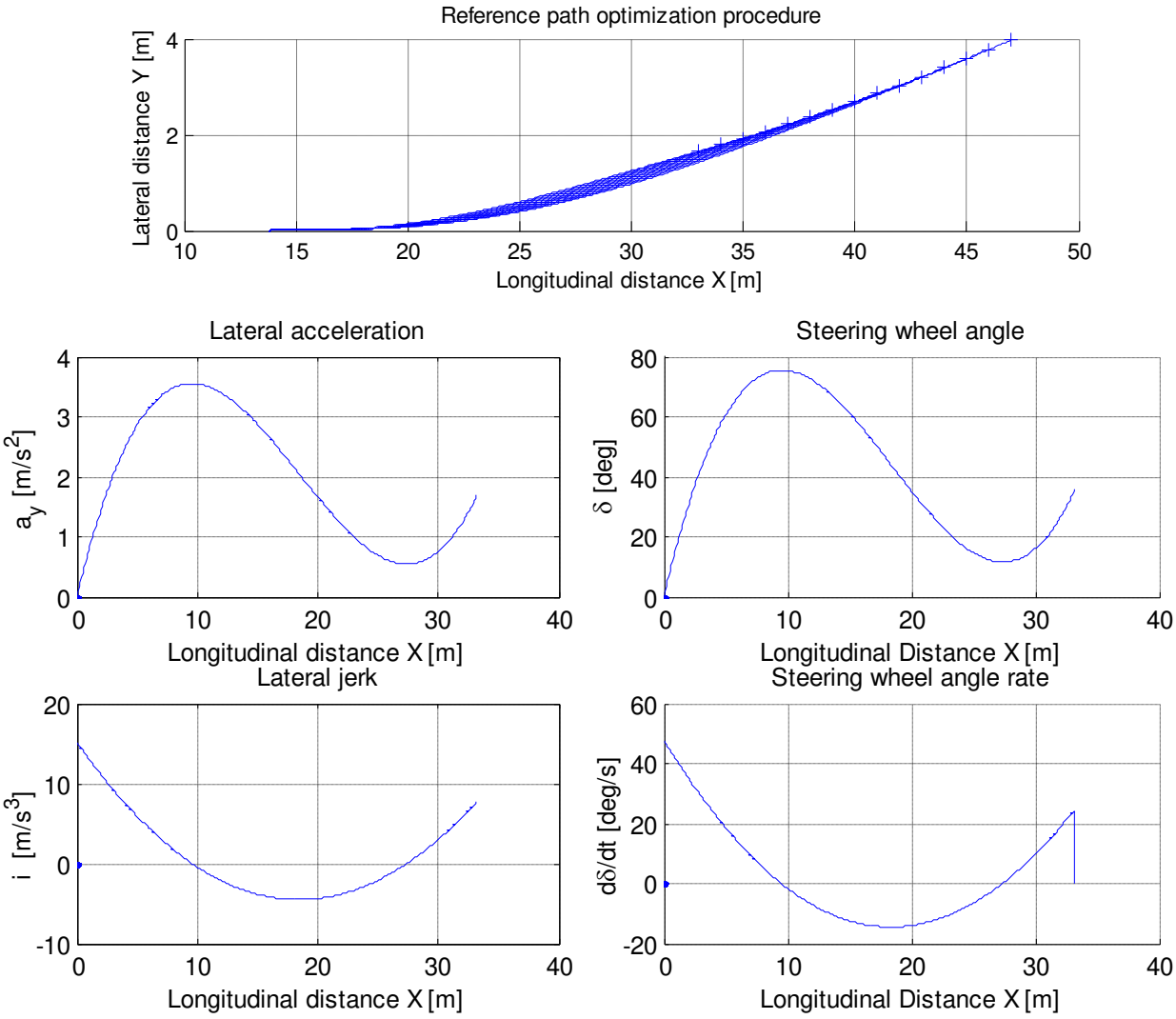

Figure 6.7 Path planning results for RORP scenario

6.1.2 Simulation results

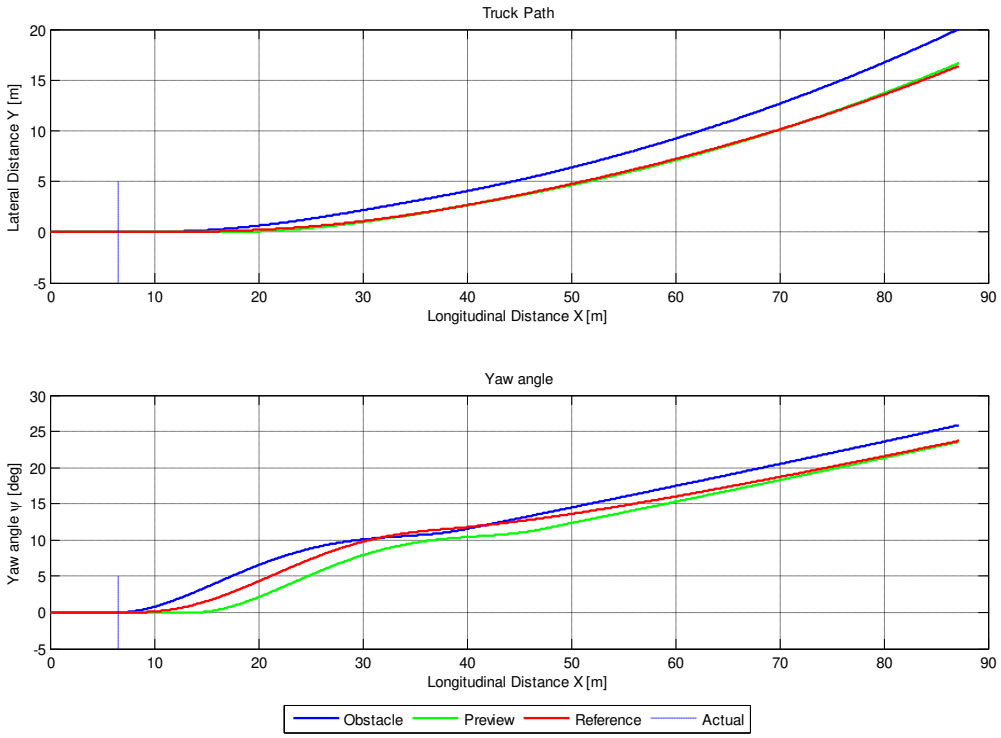

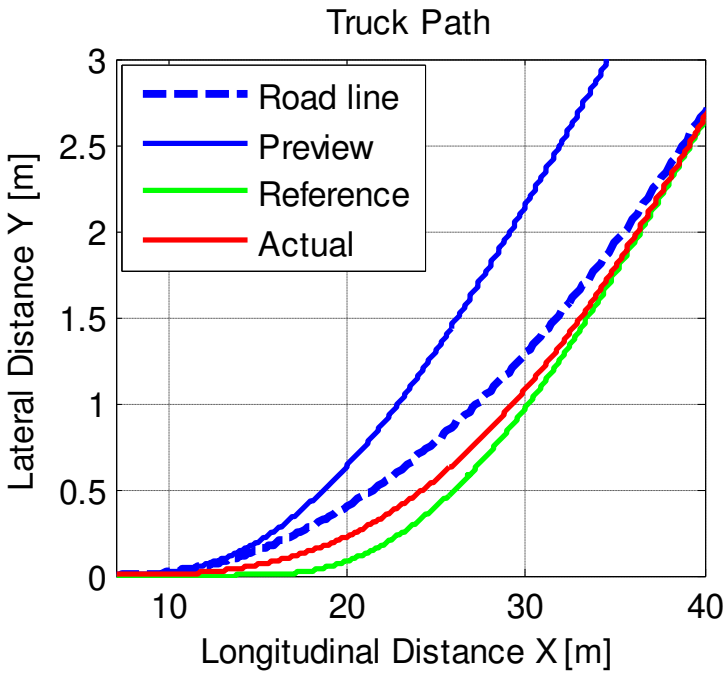

Figure 6.8 Path control results for RORP scenario- position and heading angle

It is visible in the plots that similar to previous results, the controller makes the vehicle to cut the corners therefore less lateral acceleration comparing to path planning results will be obtained.

The reason for discontinuity in jerk and steering wheel angle profile is the problem in controlling the fifth order polynomial since only the initial and final condition can be controlled while the curvature itself will not be in control. Therefore the final condition of the polynomial is changed slightly which is not exactly the initial condition for the circle as the next segment.

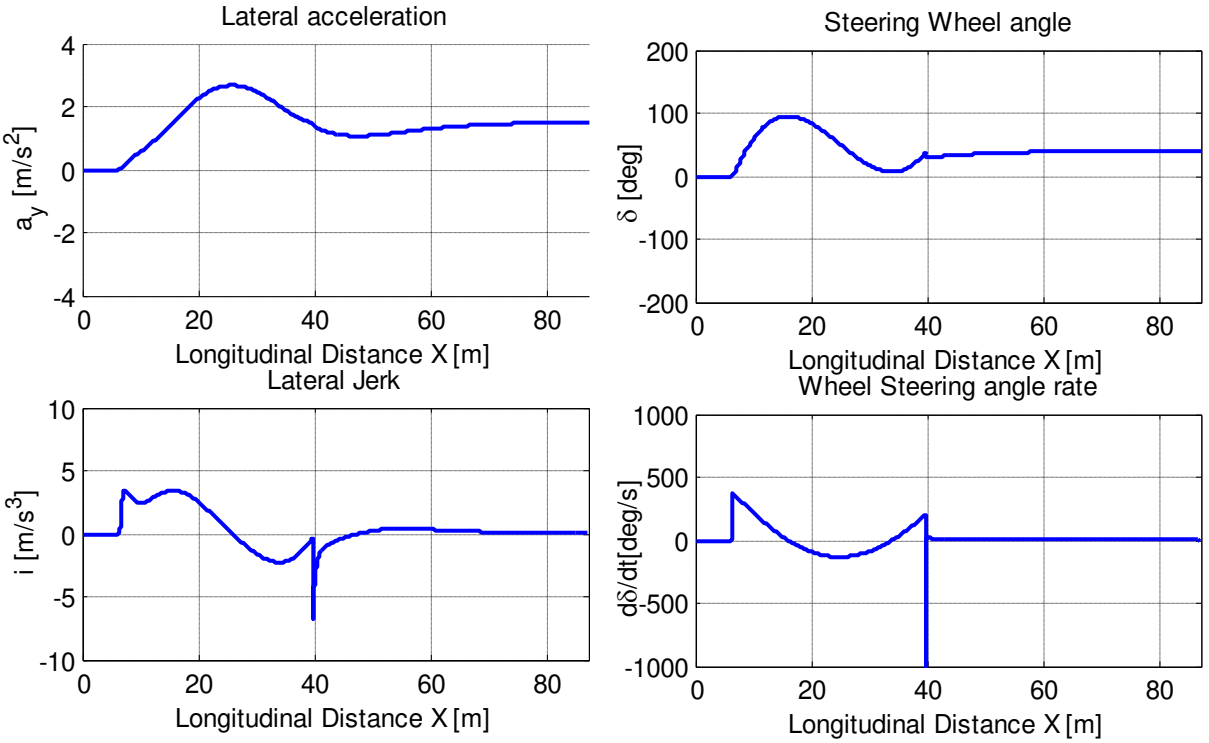

Figure 6.9 Path control results for RORP scenario-steering wheel angle and their time drivitives.

This contributes to a discontinuity at the end of polynomial curve. In order to solve this problem, a path made of smaller segments with lower order curves is recommended.

Counter steering is observed in the plots similar to previous results. The point mentioned about the peak of steering angle rate as well as the lateral jerk and torque profile also holds in this case

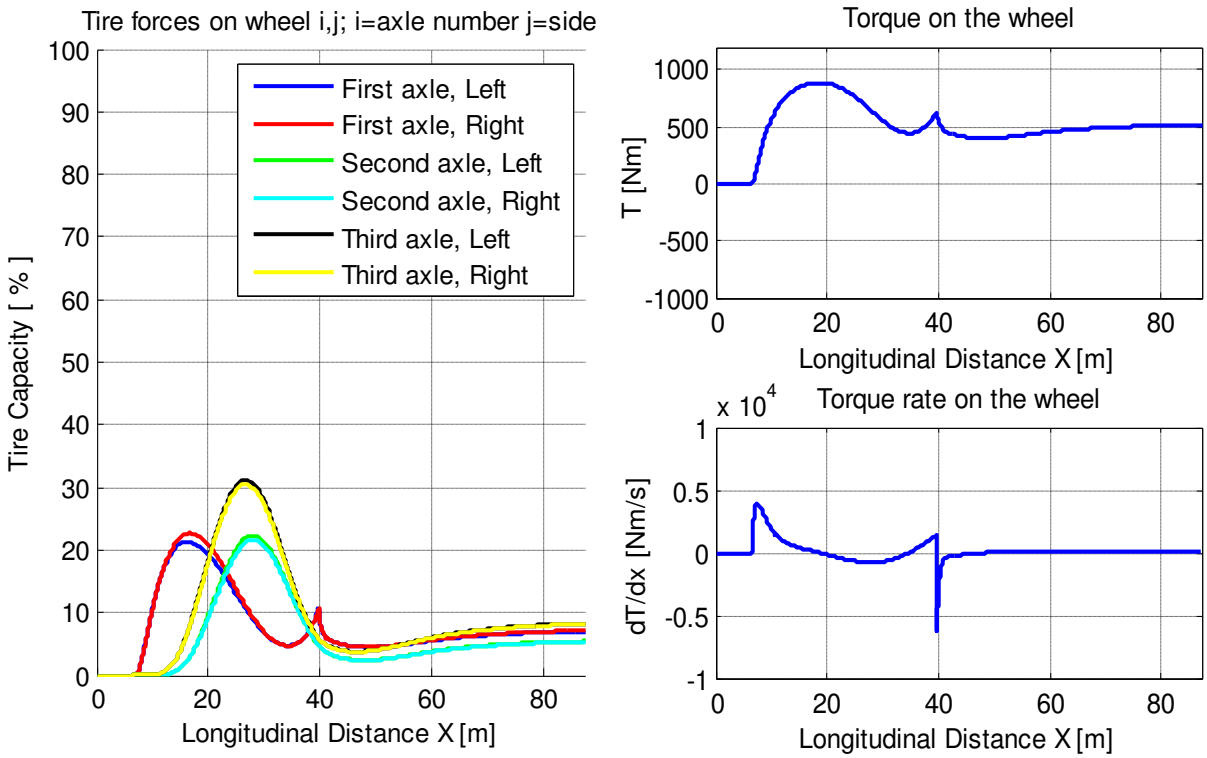

Figure 6.10 Path control results for RORP scenario tire capacity and the torque profile.

	Path error, e[m]	Heading angle error, ϵ[deg]	Handwheel angle, δ[deg]	Handwheel angle rate, $\dot{\delta}$[deg/s]	Lateral acceleration, ay[m/s^2]	Lateral jerk, i[m/s^3]	Wheel Torque T[N.m]	Wheel Torque rate $\dot{T}$[Nm/s]
max	0.29	2.24	94.69	5749.34	2.67	6.71	887.24	6167.65
@distance [m]	87.18	22.26	16.15	39.68	26.01	39.71	18.83	39.71
desired	0.10	0.01	572.95	2800.00	3.60	0.00	1150.00	0.00

Table 6.4 RORP path control simulation results.

Table 6.4 shows the results of the simulation for some parameters of interest. Maximum value for each parameter, the position of the maximum value as well as the target value and the value of the parameter at the obstacle is mentioned bellow.

The high values of steering angle rate and wheel torque rate will not be this high in implementation since they will be filtered by actuator dynamics.

7 Discussion

When the feedback control is added to feed-forward control the counter steering appears which is expected. Moreover, the peaks of steering angle is more than feed forward steering angle and this is due to the simple model used in feed forward which does not take the truck yaw dynamics into account.

The same case happens with the torque on the wheel, therefore more torque is needed on the wheel when the feedback part is added.

The lateral acceleration peak in simulation results is always lower than value coming out of path planning. The reason for this phenomenon is that on one hand the controller makes the truck to cut the sharp turns so less lateral acceleration will be obtained, on the other hand, the yaw dynamics and tire delays will act as a filter that reduces the peak of acceleration.

Regarding the plots showing the tire capacity, it can be seen that the manoeuvre is not severe. However depending on the controller gains, more of the tire capacity can be used.

It is assumed that the actuator dynamics and mechanics of the system will act as a filter for smoothening out the peaks of the steering wheel angle as well as the steering wheel angle rate and also the torque profiles.

8 Future works

- Fifth order polynomial gives the best results for the Rear End Collision while it is hard to control on Run-Off Prevention scenarios. Therefore considering the actuator filtering which allows more freedom in not having a very smooth profile, lower order curves with smaller segments is recommended for future works.
- Prediction method can be used to improve the controller efficiency. This means that the simulation can be performed for a simplified model in order to predict the vehicle behaviour before the main simulation.
- Differential braking and rear-wheel steering can be used to increase the manoeuvrability of the vehicle.
- Rotating wheels and ABS brake model can be added into the system in order to making the simulation more realistic in presence of the Brake actuator.
- Integrated steering braking interventions can be implemented to increase the stability and manoeuvrability of the vehicle.
- Rear-wheel Steering can be used to improve the manoeuvrability of the truck. The other advantage of the rear-wheel steering is reducing the front wheel steering angle and therefore less steering wheel rotation and torque which is favourable considering the driver interaction.
- Differential braking can be used during the manoeuvre for taking the car back to the path is the path error is more than a specific large value.
- Service braking at the beginning of the manoeuvre if equally distributed on the axles can improve the steering since it increases the normal force on the front axle.

APPENDIX A: Heavy Vehicle System Dynamics

Simulation of the path stability control function for the prioritized use cases requires a heavy vehicle system dynamics model. Since the integration of steering and braking for collision avoidance manoeuvre is investigated, the model needs to include both steering and braking to well provide the possibility of a handling study with path stability control.

A1. Vehicle model and relevant assumptions

For handling studies of a truck in planar motion, longitudinal and lateral displacements in addition to yaw angle are needed to study the path during manoeuvre. Relatively high centre of gravity (CG) for a truck results in a considerable amount of load transfer during different manoeuvres, therefore this requires the model to include roll angle as well. Therefore a two track four degrees of freedom (4DOF) model is needed. The model of the vehicle follows below and to complete equations of motions, forces generated by tyres will be provided in the next subsection.

A1.1 Planar free body diagram of the truck

A schematic planar sketch of the truck together with the most important tyre forces, and steering angles, are shown in Figure A. 1 using an ISO coordinate system.

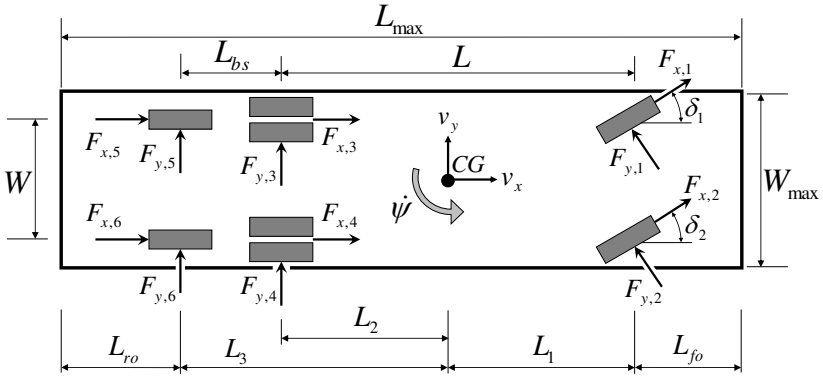

Figure A. 1 Schematic planar sketch of the 6×2 truck.

The gross dimensions L_{max} and W_{max} are particularly important for collision avoidance manoeuvres. $F_{x,n}$ and $F_{y,n}$ represent longitudinal and lateral tyre forces respectively, measured in the coordinate system fixed on the n^{th} wheel. v_x and v_y are longitudinal and lateral speed of the vehicle and $\dot{\psi}$ represents yaw rate. Finally, δ_n is steering angle of n^{th} wheel. Note that only the front axle is steered. However, wheels on other axles will also have small steer angles which are not shown but will be discussed later.

A2.1 Planar equations of motion for the truck

Since pitch dynamics and cross terms due to yaw, roll, and their time derivatives are neglected, equations of motion will be simplified as follow. In longitudinal direction (x) one can write:

$$\Sigma F_x = ma_x = m\left(\dot{v}_x - v_y\dot{\psi}\right) \qquad \text{A 1}$$

$$\Rightarrow \sum_{n=1}^{6}\left(F_{x,n}\cos\delta_n - F_{y,n}\sin\delta_n\right) = m\left(\dot{v}_x - v_y\dot{\psi}\right) \quad \text{A 2}$$

where m represents the whole mass of the truck.

In lateral direction (y) the equation will have the form below:

$$\Sigma F_y = m a_y = m\left(\dot{v}_y + v_x\dot{\psi}\right) \quad \text{A 3}$$

$$\Rightarrow \sum_{n=1}^{6}\left(F_{y,n}\cos\delta_n + F_{x,n}\sin\delta_n\right) = m\left(\dot{v}_y + v_x\dot{\psi}\right) \quad \text{A 4}$$

Finally, below equations can be written for moment in the third direction (z).

$$\Sigma M_z = I_{zz}\ddot{\psi} \quad \text{A 5}$$

$$\Rightarrow \sum_{n=1}^{6}\left(\left(F_{x,n}\sin\delta_n + F_{y,n}\cos\delta_n\right)l_n - \left(F_{x,n}\cos\delta_n - F_{y,1}\sin\delta_n\right)w_n\right) = I_{zz}\ddot{\psi} \quad \text{A 6}$$

where I_{zz} is mass moment of inertia, and l_n and w_n are longitudinal and lateral positions of n^{th} wheel in the coordinate system fixed to the body, respectively.

A3.1 Roll of the sprung mass

Roll of the sprung mass needs to be considered here because it induces lateral load transfer. Figure A. 1 shows the free body diagram of the sprung mass in dynamic equilibrium where inertial force and moment are shown in gray block arrows.

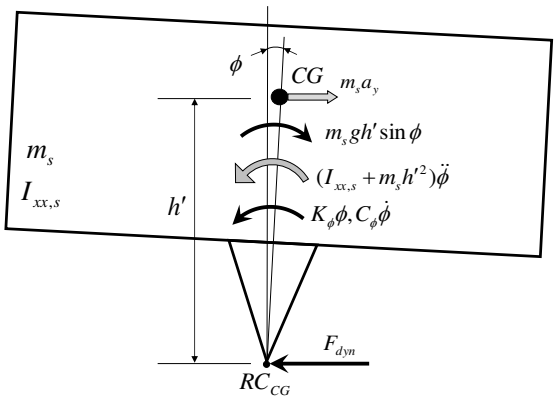

Figure A. 2 Free body diagram of the sprung mass.

The location of the centre of gravity for the sprung mass is assumed to be the same as the location of the centre of gravity for the whole vehicle since $m_s/m = 0.9 \approx 1$. Roll acceleration is calculated from differential equation expressing the roll dynamics of the sprung mass. By observing Figure A. 2, the differential equation can be derived. Note that the static equilibrium condition is taken as the reference; hence the vertical forces that balance each other are not shown. Summing the moments about the RC_{CG}, using the parallel axis theorem (Steiner theorem) and assuming small angles (roll angles do not exceed 10°):

$$\Sigma M_{RC_{CG}} = 0 \quad \text{A 7}$$

$$\left(I_{xx,s} + m_s h'^2\right)\ddot{\phi} - m_s g h'\phi + K_\phi\phi + C_\phi\dot{\phi} + m_s h'\left(\dot{v}_y + v_x\dot{\psi}\right) = 0 \quad \text{A 8}$$

A4.1 Lateral and longitudinal load transfer

Roll of sprung mass induces load transfer on all axes which can be calculated using Equation A 8 and using the free body diagram of i^{th} axle as shown in Figure A. 3. Note that the static equilibrium condition is taken as the reference; hence the vertical forces that balance each other are not shown.

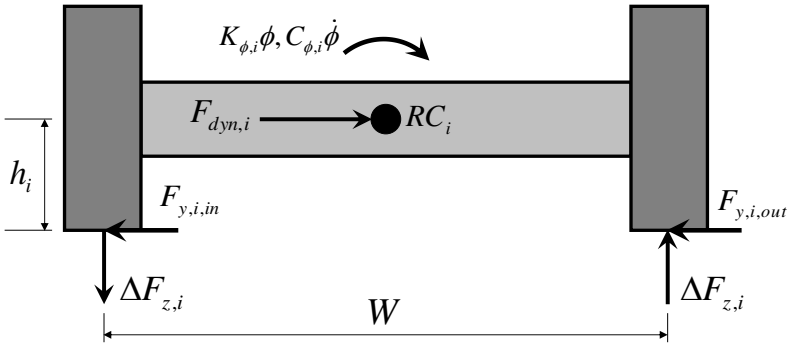

Figure A. 3 Free body diagram of the ith axle.

$F_{dyn,i}$ represents sum of the forces on the axle due to dynamical state of the axle and ignoring the mass of axle, it can be calculated as below:

$$F_{dyn,i} = F_{y,i,in} + F_{y,i,out} \qquad \text{A 9}$$

If we denote corresponding tyre to the $F_{y,i,in}$ (or $F_{y,i,out}$) with n, they can be calculated as below:

$$F_{y,i,in} = F_{x,n}\sin\delta_n + F_{y,n}\cos\delta_n \qquad \text{A 10}$$

Assuming that none of the wheels is lifted, the lateral load transfer on i^{th} axle ($\Delta F_{z,lat,i}$) could be determined by summing moments around RC_i which gives:

$$\Delta F_{z,lat,i} = \frac{C_{\phi,i}\dot{\phi} + K_{\phi,i}\phi + h_i F_{dyn,i}}{W} \qquad \text{A 11}$$

Note that additional effect of the acceleration term $\dot{\phi}h'$ on vertical forces is neglected. In order to calculate the load transfer on tandem axles, some assumptions and definitions are needed. Tandem axles are designed in a way that they prevent one axle from being overloaded and especially causing damage to the road when negotiating uneven surfaces [10]. A simple way to achieve this is to use scale-beam principle [11] where the two axles are connected to a big leaf spring and the leaf spring is mounted on the chassis in a way that it can pivot and prevent any axle in this group from losing contact with the road. On the truck of interest, this type of system is assumed. By using theoretical wheelbase (L_t) as in [12], the three-axle vehicle can be reduced to a equivalent two-axle vehicle with wheelbase equal to L_t which can be defined and calculated as:

$$L_t = L + \frac{F_{z,3,stat}}{F_{z,2,stat} + F_{z,3,stat}}\left(L_3 - L_2\right) \qquad \text{A 12}$$

where $F_{z,i,stat}$ is static load on i^{th} axle. Correspondingly, the centre of gravity from front axle can be derived as:

$$L_1 = \frac{F_{z,2,stat} + F_{z,3,stat}}{\sum_i F_{z,i,stat}} L_t \qquad \text{A 13}$$

The longitudinal load transfer can now be calculated for the equivalent 2-axle vehicle and once the total longitudinal load transfer on the tandem axle is calculated, the longitudinal load transfer on the both second and third axle could be determined by using the moment equilibrium, i.e. they are proportional to the static loads on the axles mentioned. The mathematical expressions are given as follows:

$$\Delta F_{z,lon,i}\Big|_{i=1} = -ma_x \frac{h}{L_t} \qquad \text{A 14}$$

$$\Delta F_{z,lon,i}\Big|_{i=2} + \Delta F_{z,lon,i}\Big|_{i=3} = ma_x \frac{h}{L_t} \qquad \text{A 15}$$

Using Equation A 15 and writing static equilibrium about pivot point, load transfer on tandem axles can be derived as:

$$\Delta F_{z,lon,i}\Big|_{i=2} = ma_x \frac{h}{L_t}\left(\frac{F_{z,2,stat}}{F_{z,2,stat} + F_{z,3,stat}}\right) \qquad \text{A 16}$$

$$\Delta F_{z,lon,i}\Big|_{i=3} = ma_x \frac{h}{L_t}\left(\frac{F_{z,3,stat}}{F_{z,2,stat} + F_{z,3,stat}}\right) \qquad \text{A 17}$$

Now, longitudinal load transfer on each wheel can easily be calculated dividing the load transfer on corresponding axle by the number of wheels on that axle.

In the vehicle data, the centre of gravity position is not directly given. Instead, roll centre height at each axle and the height of CG above the roll axis are provided. Here, it is assumed that the aforesaid pivot point absorbs all the lateral forces from the tyres on the second and the third axles, thus the roll centre height for the tandem axle group becomes the same as the height of the pivot point. In a typical 3-axle Volvo truck, roll centre heights at the 2nd and the 3rd axles are usually equal ($h_2 = h_3$) and therefore RC height for the tandem group is equal to one of them or the average of them. Consequently, the CG height could be calculated as:

$$h = h_1 + \left(\frac{h_2 + h_3}{2} - h_1\right)\frac{L_1}{L_t} + h' \qquad \text{A 18}$$

A5.1 Slip and net steering angles

The calculation of tyre forces does require the determination of individual slip angles at each tyre. In a two track vehicle model, track width and yaw rate induce an additional effect on the longitudinal speed of the tyre contact patch and this has to be taken into account unlike what is done in a single track (bicycle) model. The slip angles on each wheel can be calculated by the generic formula given below:

$$\alpha_n = \delta_n - \arctan\left(\frac{v_{y,n}}{|v_{x,n}|}\right) \quad , \quad n = 1,2,...6 \qquad \text{A 19}$$

The absolute value of the longitudinal speed at each wheel has to be taken since the direction of the tyre force is only determined by the direction of the lateral speed (regardless of the direction of the longitudinal speed) at each contact patch. For each

wheel, using Equation A 19, the slip angles could be written as follows (Note that the same slip angles are assumed for the tyres on the dual wheel combination on second axle):

$$\alpha_n = \delta_n - \arctan\left(\frac{v_y + l_n\dot{\psi}}{|v_x - w_n\dot{\psi}|}\right) \qquad \text{A 20}$$

In this study, only the front axle is assumed to be steerable. However, this does not mean that the steering angle for the wheels on the second and the third axles are zero. Due to the kinematics and elasticity of the axle/suspension system, wheels/axles deflect in the presence of the lateral forces, longitudinal forces, realigning moments, and sprung mass roll. The steering angles (δ_n) on all axles are determined after taking the kinematic/elastokinematic effects into consideration. Three main effects can be listed here: roll steer, lateral force steer, and aligning moment steer. Roll steer is usually the dominant effect for the trucks. It is caused by one side of the axle moving forward and the other side of the axle moving backward due to the asymmetric deflection of the leaf springs and/or the geometric location as well as the kinematics of the suspension links (including the steering links). In this study, only the roll steer is considered because of its dominance. Roll steer is normally a nonlinear function of the roll angle, but due to small roll angles, it is assumed to be a linear function of the roll angle. A roughly estimated roll steer coefficients have been acquired from [13] for the first (towards understeer), for the second (towards oversteer), and for the third axles (towards oversteer). In general, when the suspension is concerned, the wheel deflections towards toe-in are assigned to be positive (hence the roll steer coefficient is positive if the wheel deflection is towards toe-in for a positive roll angle). Note that this sign convention is used while expressing the steer angles in the report. They are given as follows for the first axle:

$$\delta_n = \delta_{r,n} + (-1)^n \varepsilon_n \phi \ , \ n = 1,2 \qquad \text{A 21}$$

where $\delta_{r,n}$ is the reduced road wheel angle of n^{th} wheel which will be discussed later. Since wheels on the tandem axles are not steered, one can calculate the wheel angle for them as below:

$$\delta_n = (-1)^n \varepsilon_n \phi \ , \ n = 3,4,5,6 \qquad \text{A 22}$$

The commanded steering wheel input is transmitted to the wheels via a recirculation ball steering gearbox and corresponding steering links. In general, the ratio between the steering wheel angle and the road wheel angle is not constant. However, here the steering ratio (i_s) is assumed to be constant and equal to 20. There are some losses while transmitting the steering wheel motion into the road wheel motion due to the elasticity on the whole steering system (including the steering column). When the tyres generate side forces, these forces "compress" the whole system, thus leading to a reduction in steer angle. The constitutive relation for this is again nonlinear, but here a linear relation is assumed. The lumped compliance for the system is taken from [13]. The expression for the "reduced" road wheel angles is given as:

$$\delta_{r,1} = \delta_{r,2} = \frac{\delta_{SWA}}{i_s} - c_\delta\left(F_{y,1} + F_{y,2}\right) \qquad \text{A 23}$$

where δ_{SWA} is steering wheel angle.

A2. Tyre model and relevant assumptions

Force generation in tyre depends on the load distribution which varies in different dynamical states of the vehicle which is due to different set of tyre forces. This load dependency in addition to tyre force saturation, gives rise to nonlinearity in tyre model. To formulate this nonlinearity in tyre model for calculation of loads on tyres, adhesion coefficient, cornering stiffness, and Magic Formula are the most important needed materials.

A6.1 Adhesion coefficient and its alteration with the vertical load

Adhesion coefficient is shown to be nonlinearly decreasing with vertical load [14]. In order to simplify this relation, it is approximated as a linear relation as below:

$$\mu_n = -\mu_{1,n} F_{z,n} + \mu_{2,n} \qquad \text{A 24}$$

Based on the values given in Table 1.3 of [15], it is assumed that the maximum adhesion coefficient at laden static load is 0.8 for all axles. It is further assumed that this value drops down to 0.75 in the presence of extreme load transfer, i.e. when the inner wheel is lifted up due to a severe manoeuvre. $\mu_{2,n}$ is taken equal to 0.85 and to emulate variations of adhesion coefficient, recalling Equation A 24 $\mu_{1,n}$ needs to be calculated as below:

$$\mu_{1,n} = \frac{0.05}{F_{z,n,stat}} \qquad \text{A 25}$$

where $F_{z,n,stat}$ represents static load on n^{th} tyre.

A7.1 Cornering stiffness and its alteration with the vertical load

The cornering stiffness, $\left(\partial F_y / \partial \alpha\right)_{\alpha=0}$, increases degressively with increase in vertical load for a pneumatic tyre. One recommendation to express this is to use a quadratic function. This function looks like as follows (for the i^{th} axle, n^{th} wheel):

$$C_{\alpha,n} = C_{1,n}\left(F_{z,n}\right)^2 + C_{2,n}\left(F_{z,n}\right) \qquad \text{A 26}$$

where $C_{1,n}$ and $C_{2,n}$ are coefficients can be found among vehicle data in Table of notations in appendix.

A8.1 Magic Formula parameters

The Magic Tyre Formula [16] is a very useful tool to model tyre forces with respect to the longitudinal slip or slip angle. It provides a "magically" good fit to the experimental tyre data, thus making it attractive to use in vehicle dynamics simulations. The mathematical expression for it is given in Equation A 27; assuming zero camber, conicity, and ply-steer.

$$F_{y,mf,n} = D_n \sin\{C_n \arctan[B_n\alpha_n - E_n(B_n\alpha_n - \arctan(B_n\alpha_n))]\} \qquad \text{A 27}$$

Note that since the longitudinal slip is not considered in the simulation, lateral tyre force versus slip angle characteristics are used in this work; hence the formulation expressing only the tyre lateral characteristics is given in Equation A 27. D, C, E, and B are parameters defining the magic formula and can be determined by trial and error

method (or using regression techniques) if the experimental tyre force versus slip angle characteristic is known. Here, all these parameters are borrowed from [16] as follow.

Peak value (D) can simply be calculated as follows:

$$D_n = \mu_n F_{z,n} \qquad \text{A 28}$$

Shape factor (C) can be calculated as:

$$C_n = 1 \pm \left(1 - \frac{2}{\pi} \arcsin\left(\frac{F_{y,a,n}}{D_n} \right) \right) \qquad \text{A 29}$$

and for curvature factor (E), one can write:

$$E_n = \frac{B_n \alpha_{m,n} - \tan\left(\frac{\pi}{2C_n} \right)}{B_n \alpha_{m,n} - \arctan\left(B_n \alpha_{m,n} \right)} \quad (\text{for } C_n > 1) \qquad \text{A 30}$$

$F_{y,a,n}$ is the lateral force vs. slip angle characteristic's horizontal asymptote, and $\alpha_{m,n}$ is the slip angle where the maximum lateral force is generated. Based on Table 1.3 of [15], the assumption of the ratio ($F_{y,a,n}/D_n = 0.75$) seems reasonable for a dry and hard surface. The slip angle where the maximum lateral force is generated ($\alpha_{m,n}$), changes directly with the vertical load. A linear function is assumed for this change (lateral shift of peak tyre force point) and the mathematical expressions used to determine $\alpha_{m,n}$ is given as in Equation A 31; the coefficients are adjusted so that the $\alpha_{m,n} = 10°$ in the vicinity of zero vertical load and $\alpha_{m,n} = 15°$ when the inner wheel is lifted up.

$$\alpha_{m,n} = \left(10 + 2.5 \frac{F_{z,n}}{F_{z0,n}} \right) \frac{\pi}{180} \qquad \text{A 31}$$

$F_{z0,i}$ is the static load on the wheel.

Stiffness factor (B_n) can now be calculated as below:

$$B_n = \frac{B_n C_n D_n}{C_n D_n} = \frac{C_{\alpha,n}}{C_n D_n} \qquad \text{A 32}$$

When a tyre generates both longitudinal and lateral force, then any of them has to be less than the adhesion limit. None of them will be equal to the adhesion limit (B_n) if this is the case. This phenomenon can be demonstrated by Kamm's circle, also known as the friction circle. This is a circle with a constant radius equal to the adhesion limit. The resultant force of the generated longitudinal and lateral force cannot exceed the circle's border. In order to take this into account, the limit side force which is denoted by "D_n" in Magic Tyre Formula is replaced by the following expression:

$$D_n \rightarrow \sqrt{D_n^2 - F_{x,n}^2} = \sqrt{\left(\mu_n F_{z,n} \right)^2 - F_{x,n}^2} \qquad \text{A 33}$$

As can be seen in the Equation A 33, a negative vertical force (usually encountered in the simulations when one wheel is lifted up due to severe cornering) will also yield a positive D_n, which will result in a lateral tyre force. Extensive attention has to be paid

on this unless roll degree of freedom of the axle is modelled in a vehicle dynamics simulation. Simulation has to be aborted when this is the case and one wheel load turns out to be negative.

Not only the lateral force, but also the longitudinal force has to be limited. When the wheel is locked due to intense braking, the whole wheel starts to slide and the force generation is altered. The wheel now acts like a solid object exposed to Coulomb friction and sliding on the road surface. This means that the resultant tyre force is parallel but in opposite direction to the sliding velocity vector at the tyre contact patch. When an excessive traction torque is applied on the wheel, the force generation is not altered because a wheel on which a traction torque is applied cannot behave like a locked wheel, i.e. absolute value of the longitudinal slip never reaches 100% unless the vehicle is fixed. Using this knowledge, the following interval can be written for the traction force:

$$-\mu_n F_{z,n} \cos\alpha_n \leq F_{x,n} \leq \mu_n F_{z,n} \qquad \text{A 34}$$

One important point here is the dependence of adhesion coefficient on the slip angle for big slip angles. Once the peak point in the tyre lateral force vs. slip angle characteristic is exceeded, the whole tread starts to slide. After this point, the more the slip angle is increased the less the adhesion coefficient becomes. This could be explained by using a Stribeck diagram [17], however the explanation is not going to be given here. When full sliding starts, then the available adhesion coefficient which will also be used to calculate the radius of the friction circle is assumed to be as follows (calculation is performed for zero longitudinal force):

$$\mu_n = \frac{\left|F_{y,mf,n}\right|}{F_{z,n}}, \text{when} \left|\alpha_n\right| > \alpha_{m,n} \qquad \text{A 35}$$

A9.1 Transient force generation

The force calculated with the Magic Tyre Formula is the steady state tyre lateral force. However, it is known that in practice, a tyre must translate in order to generate a certain amount of slip angle (generation of slip angle = generation of side force). This means that the side force build-up is not instantaneous since some time and translation distance is needed to stretch the tyre components. The required distance which is needed for the tyre to generate 63.2% of a step change in steady-state lateral force (here, this is calculated by using the Magic Formula) is defined as "relaxation length" (σ). The first order approximation for the build-up of the tyre lateral force is given as follows:

$$\frac{\sigma_{y,n}}{v_{x,n}} \dot{F}_{y,n} + F_{y,n} = F_{y,mf,n} \qquad \text{A 36}$$

where $v_{x,n}$ is the longitudinal speed at the contact patch of each wheel. Note that the differential equation above is not a linear one since $v_{x,n}$ is not constant. From [18] and [19], lateral tyre relaxation lengths for all tyres are assumed to be $\sigma_{y,n} = 0.4$ m. The same concept also applies for the longitudinal force build-up. One can write the following expression to express the gradual first order increase/decrease of the longitudinal forces. The input to the differential equation in this study is the brake forces applied by the path following controller:

$$\frac{\sigma_{x,n}}{v_{x,n}}\dot{F}_{x,n} + F_{x,n} = F_{x,rim,n} \qquad \text{A 37}$$

Note that the rim force, $F_{x,rim,n}$, is a fictitious internal force acting on the rim that results in the same tyre force in steady state. From a literature survey, one could find that the longitudinal relaxation length is roughly the half of the lateral relaxation. This could be deduced from the sample numerical values provided in [19] and [20]. Hence, the longitudinal relaxation length is assumed to be $\sigma_{x,n} = 0.2$ m for all tyres.

A3. Linear steady state cornering

In order to calculate the steering angle on the wheel for steady state cornering the equations of motion (A 1- A 6 in addition to geometrical calculations of the vehicle where all the states derivatives are considered as zero (steady state condition), are used. The steering angle calculation in steady state condition is as follows:

$$\delta = \frac{L_e}{R} + K_u \frac{a_y}{g} \qquad \text{A 38}$$

where, δ is the steering angle corresponding to the steady state condition, K_u is understeer coefficient, R is the radius of the curvature, and L_e is equivalent wheel base and can be calculated as below:

$$L_e = L + \frac{F_{z,1,static}}{F_{z,2,static} + F_{z,3,static}}(L_3 - L_2) \qquad \text{A 39}$$

A4. Rollover

Due to relatively big height of centre of gravity in a truck, it is very prone to roll over in severe manoeuvres. Therefore rollover is one of the most important issues to consider in handling studies of a heavy vehicle. To obtain a criterion for rollover, it is sufficient to keep the vehicle in steady state during the manoeuvre. This can be interpreted as having a maximum allowed lateral acceleration for the vehicle which can be calculated using the equations of motion. Using A 8 one can rewrite Equation A 11 for steady state and considering that rollover first occurs when the load transfer is equal to static load on the front outer wheel, the maximum lateral acceleration can be derived as below:

$$a_{y,\max} = \frac{WF_{z,1,stat}}{\frac{K_{\phi,1} mh'}{(K_{\phi,1} + K_{\phi,2+3}) - mh'g} + m_1 h_1} \qquad \text{A 40}$$

where, $K_{\phi,2+3}$ is the roll stiffness equivalent to the roll stiffness of the tandem axle, and m_1 is the mass distributed on the front axle.

APPENDIX B: Vehicle data

Notation	Value	Unit	Description
C_ϕ	86000	Nms/rad	Roll damping
$C_{\phi,1}$	28000	Nms/rad	Roll damping of first axle
$C_{\phi,2}$	29000	Nms/rad	Roll damping of second axle
$C_{\phi,3}$	29000	Nms/rad	Roll damping of third axle
$F_{x,n}$	-	N	Longitudinal force on n^{th} wheel
$F_{y,n}$	-	N	Lateral force on n^{th} wheel
F_{dyn}	-	N	The force corresponding to the dynamical condition
$F_{z,i,stat}$	-	N	Static load on i^{th} axle
$F_{z,n,stat}$	-	N	Static load on n^{th} wheel
I_{xx}	19000	Kgm^2	Vehicle moment of inertia around x axis
$I_{xx,s}$	-	Kgm^2	Sprung mass moment of inertia around x axis
I_{zz}	150000	Kgm^2	Vehicle moment of inertia around z axis
K_ϕ	1.54×10^6	Nm/rad	Roll stiffness
$K_{\phi,1}$	380000	Nm/rad	Roll stiffness of first axle
$K_{\phi,2}$	580000	Nm/rad	Roll stiffness of second axle
$K_{\phi,3}$	580000	Nm/rad	Roll stiffness of third axle
$K_{\phi,2+3}$	-	Nm/rad	Roll stiffness of tandem axle
L	4.900	m	Distance between the first and the second axle
L_1	3.976	m	Distance between CG and the first axle
L_2	0.924	m	Distance between CG and the second axle ($L - L_1$)
L_3	2.294	m	Distance between CG and the third axle ($L + L_{bs} - L_1$)
L_e	-	m	Equivalent wheel base;
L_{fo}	1.360	m	Front overhang
L_{max}	10.305	m	Total length of the truck
L_{ro}	2.675	m	Rear overhang ($L_{max} - L - L_{bs} - L_{fo}$)

Notation	Value	Unit	Description
L_t	5.441	m	Theoretical wheel base; Equation A 12
M_z	-	Nm	Vehicle yaw moment
W	2.050	m	Track width of the truck
W_{max}	2.495	m	Total width of the truck
X	-	m	Longitudinal position in global coordinate system
Y	-	m	Lateral position in global coordinate system
a_x	-	m/s^2	Longitudinal acceleration
a_y	-	m/s^2	Lateral acceleration
c_δ	4.88×10^{-7}	rad/N	Steering compliance
g	9.81	m/s^2	Gravitational acceleration
h	-	m	Height of centre of gravity (CG) from ground
h_1	0.3	m	Roll centre height of first axle
h_2	0.8	m	Roll centre height of second axle
h_3	0.8	m	Roll centre height of third axle
h'	0.9	m	Height of centre of gravity (CG) from roll centre (RC)
i	1,2,3	-	Index number of axles starting from front to rear
i_s	20	-	Steering gear ratio
l_n	-	m	Longitudinal position of n^{th} wheel in the coordinate system fixed to the vehicle
m	26000	kg	Vehicle mass
m_s	23500	kg	Sprung mass
m_u	2500	kg	Unsprung mass
n	1,2,...,6	-	Index number of wheels starting from front and left (1) to rear and right (6)
v_x	-	m/s	Longitudinal speed of the vehicle
v_y	-	m/s	Lateral speed of the vehicle
w_n	-	m	Lateral position of n^{th} wheel in the coordinate system fixed to the vehicle

Notation	Value	Unit	Description
$\Delta F_{z,i}$	-	N	Load transfer on i^{th} axle
α	-	rad	Slip angle
α_m	-	rad	Slip angle for which maximum lateral force is generated
δ_n		rad	Wheel angle of n^{th} wheel
ε_1	0.14	-	Roll steer coefficient of front left wheel
ε_2	0.14	-	Roll steer coefficient of front right wheel
ε_3	-0.10	-	Roll steer coefficient of dual wheels on the left
ε_4	-0.10	-	Roll steer coefficient of dual wheels on the right
ε_5	-0.10	-	Roll steer coefficient of rear left wheel
ε_6	-0.10	-	Roll steer coefficient of rear right wheel
μ_1	-	1/N	The first coefficient in adhesion calculations
μ_2	0.85	-	The second coefficient in adhesion calculations
σ_x	0.4	m	Longitudinal relaxation length
σ_y	0.2	m	Lateral relaxation length
ϕ	-	rad	Roll angle
ψ	-	rad	Yaw angle

References

1. Gerdes, J.C. and E.J. Rossetter, *A Unified Approach to Driver Assistance Systems Based on Artificial Potential Fields.* Journal of Dynamic Systems, Measurement, and Control, 2001. **123**(3): p. 431-438.
2. Hiraoka, T., O. Nishihara, and H. Kumamoto, *Automatic path-tracking controller of a four-wheel steering vehicle.* Vehicle System Dynamics: International Journal of Vehicle Mechanics and Mobility, 2009. **47**(10): p. 1205-1227.
3. Thommyppillai, M., S. Evangelou, and R.S. Sharp, *Car driving at the limit by adaptive linear optimal preview control.* Vehicle System Dynamics: International Journal of Vehicle Mechanics and Mobility, 2009. **47**(12): p. 1535-1550.
4. Kritayakirana, K. and J.C. Gerdes. *Autonomous Cornering at the Limits: Designing a Longitudinal Feedback Controller Using a Tire Slip Circle*. in *Proceedings of the 10th international symposium on advanced vehicle control*.
5. Kharrazi, S., *On Lateral Stability of Heavy Vehicle Combinations - Linking Accident Analysis and Vehicle Dynamics*. 2008, Chalmers University of Technology.
6. Yang, D., *Post Impact Vehicle Path Control in Multiple Event Accidents*. 2011, Chalmers University of Technology.
7. BILEN, Ö.B., *Path Control Algorithms for Autonomous Steering and Braking of Heavy Vehicles*. 2010, Chalmers University of Technology.
8. Mäkinen, T., et al., *Deliverable D1.5 | Use cases and requirements*. 2010.
9. Rutquist, P.E. and M.M. Edvall, *PROPT - Matlab Optimal Control Software*. 2010.
10. Heisler, H., *Advanced vehicle technology*. 2002: Butterworth-Heinemann.
11. Matschinsky, W. and A. Baker, *Road vehicle suspensions*. 2000: Professional Engineering Pub.
12. Volvo, T.C., *Volvo Truck FH 62R B3LH1 Data Sheet*. 2009.
13. Milliken, W.F. and D.L. Milliken, *Race car vehicle dynamics*. 1995: Society of Automotive Engineers.
14. Segel, L. and R.D. Ervin, *The Influence of Tire Factors on the Stability of Trucks and Tractor Trailers.* Vehicle System Dynamics: International Journal of Vehicle Mechanics and Mobility, 1981. **10**(1): p. 39-59.
15. Wong, J.Y., *Theory of ground vehicles*. 2001: John Wiley.
16. Pacejka, H.B., *Tyre and vehicle dynamics*. 2006: Butterworth-Heinemann.
17. Liang, W., J. Medanic, and R. Ruhl, *Analytical dynamic tire model.* Vehicle System Dynamics: International Journal of Vehicle Mechanics and Mobility, 2008. **46**(3): p. 197-227.
18. Ahmed, H.S.T. and H. Yarmohammadi, *Active rear wheel steering of heavy vehicles - Applied to a 6x2 Volvo truck*. 2006, Chalmers University of Technology.

19. Fancher, P., et al., *REPRESENTING TRUCK TIRE CHARACTERISTICS IN SIMULATIONS OF BRAKING AND BRAKING-IN-A-TURN MANEUVERS.* Vehicle System Dynamics: International Journal of Vehicle Mechanics and Mobility, 1997. **27**(1 supp 1): p. 207-220.

20. Klomp, M., *On Drive Force Distribution and Road Vehicle Handling - A Study of Understeer and Lateral Grip*. 2007.